Title

ELECTRONIC STRUCTURE QUANTUM MECHANICS APPLIED TO SOME SMALL POLYATOMIC MOLECULES

Author

Liskow, Dean Hemingway.

Publication Date

1974-08-01

LBL-2980
c.2

ELECTRONIC STRUCTURE QUANTUM MECHANICS APPLIED TO SOME SMALL POLYATOMIC MOLECULES

Dean Hemingway Liskow
(Ph. D. thesis)

August, 1974

Prepared for the U. S. Atomic Energy Commission
under Contract W-7405-ENG-48

DISCLAIMER

ELECTRONIC STRUCTURE QUANTUM MECHANICS APPLIED TO SOME SMALL POLYATOMIC MOLECULES

Contents

ELECTRONIC STRUCTURE QUANTUM MECHANICS APPLIED TO SOME SMALL POLYATOMIC MOLECULES

Dean Hemingway Liskow

Lawrence Berkeley Laboratory
University of California
Berkeley, California 94720

August 1974

ABSTRACT

Quantum mechanics is used to compute ab-initio wavefunctions for several molecular systems in order to derive theoretical estimates for their structure and chemical behavior. The structure of the HO_2 radical is investigated with SCF and CI wavefunctions and is predicted to have a 106.8^o bond angle. The bending potential energy for C_3, a species in carbon vapor, is investigated with SCF and CI wavefunctions and the results support the unusually low bending vibrational frequency previously determined experimentally. An SCF wavefunction is used to determine features of the $CH_3NC \rightarrow CH_3CN$ isomerization potential energy surface. And lastly, features of the $C^+ + H_2 \rightarrow CH^+ + H$ reaction potential energy surfaces are determined with CI wavefunctions.

I. INTRODUCTION

Theoretical chemists have long known that the explanation of chemical phenomena is contained in solutions to the quantum mechanical equations of motion, but only recently have they become able to produce practical solutions to these equations for systems of chemical interest, with the use of fast electronic computers and sophisticated computer programs. However, the description of chemical behavior is restricted by the level of approximation one is still forced to use to produce the quantum mechanical solution, and up to now there has been no indication that the quantum theory can not explain all the observations made experimentally. Certainly the last statement alone requires exhaustive application of the best computational methods available, but allowing that the quantum theory is correct, the computation of chemical properties can be performed to predict new phenomena and used to analyze experiments. This is the basis for the work contained in this volume.

II. BACKGROUND AND THEORY

It is now becoming a routine matter for a theoretical chemist to compute chemical properties with quantitative accuracy from first principles by using quantum mechanics, specifically the Schrödinger equation,[1]

$$H\Psi = -\frac{\hbar}{i}\dot{\Psi} \qquad (1)$$

where H is the Hamiltonian operator describing the total energy for the system under investigation, and Ψ is the wavefunction solution to the equation (1). The wavefunction Ψ may be separated into space and time parts, $\Psi(r)$ and $\phi(t)$ respectively if H is a time independent operator. This produces the equations

$$H\Psi(r) = E\Psi(r) \quad \text{and} \quad -(\hbar/i)\,\dot{\phi}(t) = E\,\phi(t). \qquad (2\text{ a and b})$$

The second equation, (2b), has the simple solution

$$\phi(t) = e^{-iEt/\hbar} \quad .$$

It is equation (2a) that is interesting since the time independent solution $\Psi(r)$ determines the total energy E and describes the structure of the system with the chosen Hamiltonian.

The Hamiltonian of interest to the chemist is just the non-relativistic electrostatic Hamiltonian for the electrons and the nuclei of a particular molecular system, given here using atomic units ($\hbar = m_e = q_e = 1$)

A,B sum over nuclei
i,j sum over electrons

$$H = \sum_A \frac{-\nabla_A^2}{2M_A} + \sum_i \frac{-\nabla_i^2}{2} + \sum_A \sum_i \frac{-Z_A}{r_{Ai}} + \sum_{A<B} \frac{Z_A Z_B}{r_{AB}} + \sum_{i<j} \frac{1}{r_{ij}} \tag{3}$$

Additional interactions[2] can be included in this Hamiltonian, but are generally treated as perturbations since the relative magnitudes of these interactions are often small compared to the electronic terms already included.

The calculation of a solution to equation (2a) using the Hamiltonian (3) which has the properties of a many electron wavefunction requires several approximations. Trial solutions are restricted to antisymmetric functions required for a many electron wavefunction by the Pauli postulate.[3] The wavefunction is determined using the variation principle, which says that a trial solution to the eigenvalue problem (2a) will have an expectation value that is always greater than the lowest eigenvalue

$$\frac{\langle \Psi_{trial} | H | \Psi_{trial} \rangle}{\langle \Psi_{trial} | \Psi_{trial} \rangle} = \langle E \rangle \geq E_{\text{lowest eigenvalue}}$$

and that the variations in Ψ_{trial} that reduce the expectation value-eigenvalue difference also reduce their error difference between Ψ_{trial} and the true ground state eigenfunction.

In practice a very common approximation used to simplify equation (2a) is the Born-Oppenheimer approximation.[4,5] This approximation involves the separation of the nuclear and electronic coordinates so that the nuclear motion is described by a potential energy surface determined for fixed nuclear positions by solving an electronic Schrödinger equation. The relationship to equation (2a) is seen where $\Psi(r)$ is assumed to factor into electronic and nuclear parts

$$\Psi(r) = \Psi_R(r_e)\ \phi(R), \qquad r_e = \text{electronic coordinates}$$
$$R = \text{nuclear coordinates.} \qquad (4)$$

where the subscript on $\Psi_R(r_e)$ signifies that the electronic wavefunction depends parametrically on the nuclear coordinates. If nuclear and electronic terms in the Hamiltonian are collected together in the resulting equation one obtains

$$-\frac{1}{2}\sum_A \frac{1}{M_A}\left[\Psi_R(r)\nabla_A^2\ \phi(R) + (\nabla_A\Psi_R(r)).\ (\nabla_A\phi(R)) + \phi(R)\nabla_A^2\Psi_R(r)\right]$$
$$-\frac{1}{2}\sum_i \phi(R)\nabla_i^2\Psi_R(r) + \left(\sum_A\sum_i \frac{-Z_A}{r_{Ai}} + \sum_{A<B}\frac{Z_A Z_B}{R_{AB}} + \sum_{i<j}\frac{1}{r_{ij}}\right)\Psi_R(r)\phi(R)$$
$$= E\ \Psi_R(r)\phi(R). \qquad (5)$$

If the last two terms in the square brackets are dropped, the separated equations that result are

$$-\frac{1}{2}\sum_i \nabla_i^2\Psi_R(r) + \left(\sum_{Ai}\frac{-Z_A}{r_{Ai}} + \sum_{A<B}\frac{Z_A Z_B}{R_{AB}} + \sum_{i<j}\frac{1}{r_{ij}}\right)\Psi_R(r) = E(R)\Psi_R(r) \qquad (6a)$$

and

$$- \frac{1}{2} \sum_A \frac{1}{M_A} \nabla_A^2 \phi(R) = (E - E(R))\phi(R) \quad . \tag{6b}$$

Equation (6a) corresponds to the electronic Schrödinger equation mentioned earlier, and (6b) is a Schrödinger equation for the nuclei using the potential energy surface E(R). It is a requirement for the validity of this approximation that the two neglected terms really be insignificant. The fact that these terms are weighted by the reciprocal of the nuclear mass usually provides the required smallness since the terms inside the brackets are of the same magnitude as the purely electronic terms.[6]

The next approximation is the most severe approximation involved in ab-initio calculations today. That is the use of a finite basis set for expanding solutions to the Schrödinger equation. Basis set expansion is desirable because the eigenvalue problem is reduced to a matrix algebra problem, but selection of a basis set not only is costly in terms of variational energy but it also introduces arbitrariness into the calculation. However, much work has been done to categorize and produce standardized basis sets[7] capable of reliable application to molecular calculations. In addition to reliability, the basis functions should also be of a form that allows convienient application to molecular systems. The expoential or Slater[8] type basis function (in spherical coordinates)

$$\phi = C\, r^{n-1} e^{-\zeta r} Y_{\ell m}(\theta,\phi)$$

has the desired asymptotic behavior for the wavefunction, but is unsuited for the computation of multicenter two-electron integrals resulting from the $1/r_{ij}$ term in the molecular Hamiltonian (3). Slater basis functions have been economical only for atoms and linear molecules. The Gaussian basis function[9] (in cartesian coordinates)

$$\phi = C\, X^n Y^m Z^\ell\, e^{-\alpha r^2}$$

does not have the proper asymptotic behavior for a solution to (6a) like Slater functions have, but Gaussian functions can be efficiently[10] incorporated in multicenter two-electron integrals. This efficiency allows an increase in the basis set size, so that a variational calculation performed with Gaussian functions can be made comparable in energy to a particular Slater basis calculation, and still involve much less computation than the corresponding Slater basis calculation.[11]

The trial wavefunction to be made into an approximate solution to (6a) via the variational principle must be antisymmetric. The antisymmetric requirement is a result of the Pauli postulate[3] which requires that a many-electron wavefunction be antisymmetric for interchange of the coordinates of any two electrons. In the case where the many-electron wavefunction is to be approximated by the product of one-electron functions, the antisymmetry requirement is satisfied by using a Slater determinant.[12] The best wavefunction in a variational sense consisting of only one determinant is called the Hartree-Fock wavefunction. However, in general, a single determinant will not be a simultaneous eigenfunction of operators commuting with the Hamiltonian in (6a), and the wavefunction will have to be minimally constructed for several determinants.[13] This minimal multi-determinant wavefunction constructed to be a simultaneous eigenfunction for all the commuting operators (i.e. symmetry and spin operators) is called a single configuration.

One way of constructing a many-electron wavefunction is the self-consistent field (SCF) method where the one-electron functions (called orbitals) are redetermined variationally until the orbitals no longer change. Roothaan[14] has developed the SCF theory for Hartree-Fock wavefunctions using orbitals expanded in finite basis sets. However, even the exact Hartree-Fock wavefunction fails to account for the electron correlation due to instantaneous electron-electron repulsion. The correlation error can, in principle, be accounted for by using a multiconfiguration wavefunction[15]

$$\Psi(r) = \sum_i C_i \Psi_i(r)$$

also called a configuration interaction (CI) wavefunction,[16] where C_i is the expansion coefficient for the <u>ith</u> configuration $\Psi_i(r)$. The CI wavefunction is calculated by variationally determining the configuration expansion coefficients, a matrix eigenvalue problem; but unless the expansion contains all configurations possible (a full CI) for the basis set used, the choice of orbitals will still affect the calculated energy.[2] Since a full CI calculation is only practical for a small basis set, the orbitals must be optimized when they are used in an incomplete CI calculation. The selection of configurations and orbitals in this case is another arbitrary element entering the wavefunction, and has been the motivation for several theoretical approaches[17-19] designed to select the most important configurations and orbitals.

REFERENCES

1. E. Schrödinger, Ann. Physic. 79, 361, 489, 734; 81, 109 (1926), Phys. Rev. 28, 1049 (1926).
2. R. McWeeny and B. T. Sutcliffe, Methods of Molecular Quantum Mechanics, Academic Press, London, 1969.
3. W. Pauli, Phys. Rev. 58, 716 (1940).
4. M. Born and R. Oppenheimer, Ann. Physic. 84, 457 (1927).
5. G. Herzberg, Molecular Spectra and Molecular Structure, III. Electronic Spectra and Electronic Structure of Polyatomic Molecules, Van Nostrand Reinhold Co., New York, 1966.
6. F. L. Pilar, Elementary Quantum Chemistry, McGraw-Hill, New York, 1968.
7. H. F. Schaefer, III, The Electronic Structure of Atoms and Molecules, A Survey of Rigorous Quantum Mechanical Results, Addison-Wesley, Reading, Massachusetts, 1972.
8. J. C. Slater, Phys. Rev. 36, 57 (1930).
9. S. F. Boys, Proc. Roy. Soc. (London), A200, 524 (1950).
10. I. Shavitt, "The Gaussian Function of Calculations of Statistical Mechanics and Quantum Mechanics," in Methods in Computational Physics, Vol. 2, Academic Press, New York, (1963).
11. R. P. Hosteny, T. H. Dunning, R. R. Gilman, A. Pipano, and I. Shavitt, Chem. Phys. Letters 7, 325 (1970).
12. J. C. Slater, Phys. Rev. 34, 1293 (1929).
13. P.-O. Löwdin, Advan. Chem. Phys. 2, 207 (1959).

14. C. C. J. Roothaan, Rev. Mod. Phys. 23, 696 (1951); Rev. Mod. Phys. 32, 179 (1960).

15. P.-O. Löwdin, Phys. Rev. 97, 1474 (1955).

16. R. K. Nesbet, Proc. Roy. Soc. A230, 312 (1955).

17. G. Das and A. C. Wahl, J. Chem. Phys. 44, 876 (1966), 47, 2934 (1967), Phys. Rev. Letters 24, 440 (1970), Advan. Quantum Chem. 5, 261 (1970).

18. H. F. Schaefer III and F. E. Harris, Phys. Rev. Letters 21 1561 (1968), H. F. Schaefer, III, R. A. Klemm, and F. E. Harris, Phys. Rev. 181, 137 (1969).

19. A. D. McLean and B. Liu, J. Chem. Phys. 58, 1066 (1973).

III. APPLICATIONS IN CHEMICAL SYSTEMS

This section deals with the application of quantum mechanics to systems of chemical interest.

A. HO_2 - Geometry Determination of a Radical Intermediate

1. Preliminaries

The hydroperoxyl radical, HO_2, is found as an intermediate species generated by several important reaction systems. Direct investigation of HO_2 in the laboratory is hampered by its short lifetime and consequent small concentrations. It was first observed in a mass spectrometer by Foner and Hudson[1] and confirmed by several later investigations.[2-4] However, more detailed spectroscopic investigations of HO_2 waited until Milligan and Jacox[5] and then Ogilvie[6] observed HO_2 absorption using matrix isolation techniques. Continued experimental investigation has produced much more data on HO_2. Paukert and Johnston[7] applied molecular modulation spectroscopy, a technique especially adapted to investigation of intermediates, to HO_2 and measured kinetic rate constants and the gas phase absorption spectrum. Hochanadel, Gormley, and Ogren[8] reported additional work on the kinetics of HO_2 using flash photolysis. Recently Radford, Evenson, and Howard[9] detected some far infrared rotational transitions using laser magnetic resonance (LMR) on HO_2. And lastly, Hunziker and Wendt[10] measured the absorption spectrum in the near infrared while Becker, Fink, Langen, and Schurath[11] measured the same region for emission.

Paukert and Johnston[7] report vibrational frequencies at 1095, 1390, and 3410 cm^{-1} measured from a gas phase sample, and in essential agreement with the matrix isolation experiments.[5,6] This experimental evidence indicates that HO_2 has two inequivalent oxygen atoms, but there is insufficient data to determine the geometry with precision. Paukert and Johnston claim only that their spectrum is consistent with the geometry $\angle HOO = 108^{\circ}$, R(H-O) = 0.96 Å, and R(O-O) = 1.28 Å, estimated from the known geometry of O_2, H_2O_2, H_2O and with the use of Walsh's rules[12] to determine the angle. Walsh theorized that ground state HO_2 should be bent with an angle only slightly smaller than HNO (The HNO angle measured by Dalby[13] is 108.5° for the $^1A'$ ground state). Figure 1 shows a Walsh diagram for the HAB system illustrating Walsh's prediction for HO_2. Hunziker and Wendt[11] report an estimate of 1.41 ± 0.03 Å for the HO_2 ground state O-O distance based on their absorption spectrum and Badger's rule.

2. Basis Set and Wavefunction

This work[14] was designed to provide *ab-initio* theoretical evidence for the structure of HO_2 with quantitative accuracy. Previous calculations[15] on small molecules have shown the effects basis set size and the treatment of electron correlation on calculated molecular geometry. So a slightly better than "double zeta" basis set of contracted gaussian functions is used for HO_2. For the hydrogen atom Huzinaga's five gaussian basis set[16] is contracted to three functions, and on each oxygen atom Huzinaga's (9s5p) basis[16] is contracted to form a (4s2p) basis by using Dunning's contraction scheme.[17] Table I shows the final basis set and contraction scheme used for HO_2. Table II shows the symmetry grouping into 19a' and 4a" basis functions for the C_2 molecular symmetry.

Choosing the configurations for describing the electron correlation was done with the first-order wavefunction[18,19] method. This method is designed to select configuration types required to account for most of the valence electron correlation corrections to an SCF or Hartree-Fock wavefunction. For the HO_2 system the Hartree-Fock configuration is

$$1a'^2\ 2a'^2\ 3a'^2\ 4a'^2\ 5a'^2\ 6a'^2\ 7a'^2\ 1a''^2\ 2a''^1\ (^2A''). \quad (1)$$

Table III lists the 500 configurations selected for an approximate first order wavefunction calculation for HO_2. This configuration list is the result of additional simplifications to reduce the total number of configurations. One simplification is not allowing excitations from the 3a' and 4a' orbitals which, if included, would increase the total to 1086 configurations. The other simplification added to the first order method is to delete the 9a' orbital from the valence orbitals given special treatment in the first order selection scheme. Inclusion of the 9a' orbital with the valence orbitals would make a total of 803 configurations, and without either simplification there would be 1837 configurations. Upon closer inspection, these simplifications needed for economy can be justified since the 3a' and 4a' orbitals correspond to the oxygen 2s atomic orbitals and the 9a' orbital corresponds to a $3\sigma_u$ orbital for O_2 when R(O-O) is near the equilibrium position. This $3\sigma_u$ orbital has been found[20] to be unimportant for O_2 when R(O-O) is in the equilibrium region.

Calculations are performed for both HO_2 and O_2 using the same basis set and configuration selection methods. The calculational procedure in each case starts with an SCF calculation to determine the best one-electron functions or orbitals occupied in the Hartree-Fock configuration. This is done by annihilation of single excitation configurations, and transforming the orbitals to canonical form. The remaining unoccupied orbitals are constructed to describe excited states of HO_2^+ and O_2^+. This exhausts the basis set and provides starting orbitals more suited for use in an incomplete CI calculation because core orbitals are energetically separated from valence and higher orbitals. This separation helps to justify the unequal treatment given to valence orbitals with respect to core and higher orbitals in selection of configurations. Next, these starting orbitals are replaced by the natural orbitals[21] determined from the first order CI wavefunction. Natural orbital are produced iteratively[22] by repeated first order CI stages until the total energy stabilizes or increases slightly.

3. Result and Analysis

Paukert and Johnston's estimate for the geometry of HO_2 was used to choose a grid of geometry points for calculating the three dimensional potential energy surface. The SCF and first order CI energies calculated are given in Table IV. The number of calculation points is small because of the expense of the calculation (15 minutes a point on a CDC 6600 computer). The surfaces were then fit to the quadratic form

$$E = E_o + K_{OH}(r(OH) - r_e(OH))^2 + K_{OO}(r(OO) - r_e(OO))^2 + K_\theta(\theta-\theta_e)^2\ r_e(OO)\ r_e(OH) \tag{2}$$

by least squares minimization. The quadratic potential parameters are listed in Table V for both the SCF and CI wavefunctions.

The accuracy of the calculated geometric parameters can be estimated from the O_2 results in comparison with experimental measurements and with other calculations. Experimentally[23] the O_2 bond is 1.207 Å long and has a force constant of 11.8 mdyn/Å, while the calculations show 1.205 Å and 16.35 mdyn/Å for the SCF wavefunction and 1.270Å and 10.25 mdyn/Å for the first order CI wavefunction. Past first order calculations[20] on O_2 using a more extended basis set (d functions) yield better agreement with experiment. It is usual for extended basis set calculations to reduce calculated bond lengths, and for O_2 the Hartree-Fock bond length is 1.152 Å.[24] This indicates that the SCF geometry calculated here is likely to be more accurate than the CI results because of the basis set size used.

The geometry calculated for HO_2 should show the same trends as O_2 with respect to the chosen basis set. This means that the SCF bond lengths, r(OH) = 0.986 Å and r(OO) = 1.384 Å, should be closer to experiment than the CI results, r(OH) = 0.973 Å and r(OO) = 1.458 Å. In both calculations, the bond angle should be reliable. The SCF angle is 106.8° and the CI angle is 104.6°, both near the angle rationalized by the Walsh method.

The O-O bond on HO_2 is not like the bond in O_2; it is longer and has a weaker force constant near equilibrium. The O-O bond length in HO_2 is nearer to that of H_2O_2 where r(O O) = 1.475 Å. The O-O force constants calculated for HO_2 are 4.65 mdyn/Å for the SCF potential and 2.51 mdyn/Å for the CI potential, while the O-O force constant in H_2O_2 is 4.01 mdyn/Å[25] and in O_2 it is 11.8 mdyne/Å.[23] This also indicates that the O-O bond is like that in H_2O_2. The calculated O-O bond force constants for HO_2 show a factor of two difference between the SCF and CI wavefunctions. When using the same basis set a CI wavefunction gives a description of the electronic structure in a form allowing the wavefunction to correctly dissociate to atoms and fragments. This means that force constants should be more reliable for CI than SCF wavefunctions within a given basis set, and the force constant typically has a lower value for the CI wavefunction.

The hydrogen atom dissociation energy for HO_2 is calculated from the difference of the HO_2 and O_2 + H total energies. The SCF calculation yields a value D_e = 2.36 eV and the CI calculation a value of D_e = 1.85 eV compared to the experimental value of D_e = 2 eV found by Foner and Hudson.[4]

The electron correlation introduced with the CI wavefunction can be examined by observing the natural orbital occupation numbers[21] for the wavefunction. These numbers are listed in Table VI for the geometry with the lowest calculated energy for each of HO_2 and O_2. The occupation numbers are integers for the single configuration SCF wavefunction, and the difference from integer values found in the CI occupation numbers is a measure of the added correlation.

The 500 configuration first order wavefunction for HO_2 has 200 different orbital occupancies, but only a few of these occupancies produce most of the improvement found with the CI wavefunction. Table VII lists the ten most important occupancies for HO_2 selected by the energy criterion

$$E = \sum_i C_i^2 (H_{ii} - H_{11})$$

where H_{ii} is the diagonal Hamiltonian matrix element for the ith configuration associated with the chosen occupancy, C_i is the CI expansion coefficient for the ith configuration, and H_{11} is the dominant diagonal Hamiltonian matrix element. The 8a' and 2a" orbitals are seen to be involved in most of the important configurations listed in Table VII.

REFERENCES

1. S. N. Foner and R. L. Hudson, J. Chem. Phys. 21, 1608 (1953).

2. A. J. Robertson, "Applied Mass Spectroscopy," Inst. of Petroleum, London, 1954.

3. K. U. Ingold and W. A. Bryce, J. Chem. Phys. 24, 360 (1956).

4. S. N. Foner and R. L. Hudson, J. Chem. Phys. 36, 2681 (1962).

5. D. E. Milligan and M. E. Jacox, J. Chem. Phys. 38, 2627 (1963). 40, 605 (1964).

6. J. F. Ogilvie, Spectrochim. Acta, Part A, 23, 737 (1967).

7. T. T. Paukert and H. S. Johnston, University of California Radiation Laboratory, Report No. UCRL-19109, Nov. 1969.

8. C. J. Hochanadel, J. A. Ghormley, and P. J. Ogren, J. Chem. Phys. 56, 4426 (1972).

9. H. F. Radford, K. M. Evenson, and C. J. Howard, J. Chem. Phys 60, 3178 (1974).

10. H. E. Hunziker and H. R. Wendt, J. Chem. Phys. 60, 4622 (1974).

11. K. H. Becker, E. H. Fink, P. Langen, and U. Schurath, J. Chem. Phys. 60, 4623 (1974).

12. A. D. Walsh, J. Chem. Soc. 2288 (1953).

13. F. W. Dalby, Can. J. Phys. 36, 1336 (1958).

14. D. H. Liskow, H. F. Schaefer, III, and C. F. Bender, J. Am. Chem. Soc. 93, 6734 (1971).

15. H. F. Schaefer, III, The Electronic Structure of Atoms and Molecules: A Survey of Rigorous Quantum Mechanical Results, Addison-Wesley, Reading, Massachusetts, 1972.

16. S. Huzinaga, J. Chem. Phys. 42, 1293 (1965).

17. T. H. Dunning, Jr. J. Chem. Phys. 53, 2823 (1970).

18. H. F. Schaefer, III, and F. E. Harris, Phys. Rev. Letters 21, 1561 (1968).

19. C. F. Bender and H. F. Schaefer, III, J. Chem. Phys. 54, 1720 (1971).

20. H. F. Schaefer, III, J. Chem. Phys. 54, 2207 (1971).

21. P.-O. Löwdin, Phys. Rev. 97, 1474 (1955).

22. C. F. Bender and E. R. Davidson, J. Phys. Chem. 70, 2675 (1966).

23. G. Herzberg, Spectra of Diatomic Molecules, Van Nostrand, Princeton, N. J., 1950.

24. P. E. Cade, unpublished work.

25. R. L. Redington, W. B. Olson, and P. C. Cross, J. Chem. Phys. 36, 1311 (1962).

Table I. Basis Set[a] and Contraction.[b]

	Gaussian exponent	Contraction coefficient
Oxygen		
s	7816.54	0.002031
	1175.82	0.015436
	273.188	0.073771
	81.1696	0.247606
	27.1836	0.611832
	3.4136	0.241205
	9.5322	1.0
	0.9398	1.0
	0.2846	1.0
p	35.1832	0.019580
	7.9040	0.124189
	2.3051	0.394727
	0.7171	0.627375
	0.2137	1.0
Hydrogen		
s	33.640	0.025374
	5.0580	0.189684
	1.1470	0.852933
	0.3211	1.0

Table I (continued

	Gaussian exponent	Contraction coefficient
Hydrogen		
s	0.1013	1.0

[a]Ref. 16

[b]Ref. 17

Table II. Basis Function Symmetry.

Atom	Function	C_s symmetry $\underline{a'}$	$\underline{a''}$
O(1)	s	4	
	p_x	2	
	p_y	2	
	p_z		2
O(2)	s	4	
	p_x	2	
	p_y	2	
	p_z		2
H	s	3	
Total		19	4

Table III. Configurations in the Approximate First-Order Wave Functions for the $^2A''$ State of HO_2[a]

Type excitation	$^2A''$ config per orbital occupancy	Total config
$1a'^2 2a'^2 3a'^2 4a'^2 5a'^2 6a'^2 7a'^2 1a''^2 2a''$	1	1
5a′, 6a′, 7a′ → 8a′, 9a′, . . . , 19a′	2	72
1a″ → 2a″, 3a″, 4a″	2	6
2a″ → 3a″, 4a″	1	2
$5a'^2, 6a'^2, 7a'^2 \rightarrow 8a'^2$	1	3
$5a'6a', 5a'7a', 6a'7a' \rightarrow 8a'^2$	2	6
5a′1a″, 6a′1a″, 7a′1a″ → 8a′2a″	2	6
$1a''^2 \rightarrow 8a'^2$	1	1
$1a''2a'' \rightarrow 8a'^2$	1	1
$5a'^2, 6a'^2, 7a'^2, 1a''^2 \rightarrow$ 8a′9a′, . . . , 8a′19a′	2	88
$5a'^2, 6a'^2, 7a'^2, 1a''^2 \rightarrow$ 2a″3a″, 2a″4a″	1	8
5a′6a′, 5a′7a′, 6a′7a′ → 8a′9a′, . . . , 8a′19a′	5	165
5a′6a′, 5a′7a′, 6a′7a′ → 2a″3a″, 2a″4a″	2	12
1a″2a″ → 8a′9a′, . . . , 8a′19a′	2	22
5a′1a″, 6a′1a″, 7a′1a″ → 8a′3a″, 8a′4a″	5	30
5a′1a″, 6a′1a″, 7a′1a″ → 9a′2a″, . . . , 19a′2a″	2	66
5a′2a″, 6a′2a″, 7a′2a″ → 8a′3a″, 8a′4a″	2	12
Total		500

[a] Most orbital occupancies give rise to more than one linearly independent doublet ($S = 1/2$) spin eigenfunctions. For a discussion of spin eigenfunctions, see R. Pauncz, "Alternate Molecular Orbital Theory," W. B. Saunders, Philadelphia, Pa., 1967.

XBL 748-1411

Table IV. Calculated HO_2 Energies (Hartrees) and Bond Distances (Bohrs)[a]

r(H-O)	r(O-O)	θ	SCF	First order
1.8	3.0	110	−150.13520	−150.23546
1.8	2.8	110	−150.15090	−150.24299
1.8	2.4	110	−150.15009	−150.22473
2.0	2.6	110	−150.14961	−150.23471
1.6	2.6	110	−150.14331	−150.22656
1.8	2.6	120	−150.15293	−150.23641
1.8	2.6	100	−150.15621	−150.24138
1.8	2.6	110	−150.15834	−150.24237
1.8	2.8	100	−150.15140	−150.24445
1.8	2.8	90	−150.14427	−150.23934
1.8	3.0	100	−150.13744	−150.23915
2.0	2.8	100	−150.14302	−150.23701
1.8	2.9	100	−150.14525	−150.24211

[a] 1 hartree = 27.21 eV; 1 bohr = 0.5292 Å.

XBL 748-1412

Table V. Geometries and Force Constants for HO_2 and O_2.

Property	SCF(HO_2)	SCF(O_2)	CI(HO_2)	CI(O_2)	Exp. (OH)	Exp. (O_2)	Exp. (H_2O_2)	Exp. (H_2O)
Minimum Energy (Hartree)	-150.1579	-149.5712	-150.2448	-149.6768				
O-H Bond Length Å	0.968	---	0.973	---	0.97[a]			
O-O Bond Length Å	1.384	1.205	1.458	1.270		1.207[a]	1.475[b]	
Bond Angle (deg.)	106.8	---	104.6	---			94.8[b]	
k(OH) (mdyn/Å)	8.49	---	8.56	---	7.8[a]	---	7.81[b]	8.4[c]
k(OO) (mdyn/Å)	4.65	16.35	2.51	10.25	---	11.8[a]	4.010[b]	---
k(θ) (mydn/Å)	0.61	---	0.47	---	---	---	0.8[b]	0.76[c]

[a]Ref. 23

[b]Ref. 25

[c]J. W. Nibler and G. C. Pimentel, J. Mol. Spectrosc. 25, 240 (1968).

Table VI. Natural Orbital Occupation Numbers of HO_2 and O_2

Orbital	HO_2	Orbital	O_2
1a'	2.0	$1\sigma_g$	2.0
2a'	2.0	$1\sigma_u$	2.0
3a'	2.0	$2\sigma_g$	2.0
4a'	2.0	$2\sigma_u$	2.0
5a'	1.996	$3\sigma_g$	1.971
6a'	1.991	$3\sigma_u$	0.0283
7a'	1.931	$4\sigma_g$	0.0003
8a'	0.0728	$4\sigma_u$	0.0001
9a'	0.0065		
10a'	0.0032	$1\pi_u$	3.924
11a'	0.0003	$1\pi_g$	2.060
		$2\pi_u$	0.0114
1a"	1.974	$2\pi_g$	0.0028
2a"	1.017		
3a"	0.0065		
4a"	0.0019		

Table VII. Important Configurations in the Approximate First-Order Wave Function for HO_2. The Geometry Is r(H–O) = 1.80, r(O–O) = 2.80, θ = 100°

	Excitation	Coefficient	Energy criterion, hartrees
1.	$1a'^2 2a'^2 3a'^2 4a'^2 5a'^2 6a'^2 7a'^2 1a''^2 2a''$	0.9709	
2.	$7a'^2 \longrightarrow 8a'^2$	0.1419	0.0226
3.	$7a'1a'' \longrightarrow 8a'2a''$	0.1252	0.0153
4.	$6a'7a' \longrightarrow 8a'9a'$	0.0683	0.0082
5.	$5a'7a' \longrightarrow 8a'10a'$	0.0474	0.0043
6.	$1a'' \longrightarrow 3a''$	0.0516	0.0032
7.	$7a'2a'' \longrightarrow 8a'3a''$	0.0313	0.0030
8.	$7a'1a'' \longrightarrow 8a'3a''$	0.0396	0.0027
9.	$6a'1a'' \longrightarrow 9a'2a''$	0.0408	0.0022
10.	$7a'1a'' \longrightarrow 8a'4a''$	0.0305	0.0021

XBL 748-1413

FIGURE CAPTION

Fig. 1. Walsh diagram for the HO_2 system. Electron occupancy, depicted by small arrows, indicates that a bent geometry is favored because the 7a' orbital is occupied.

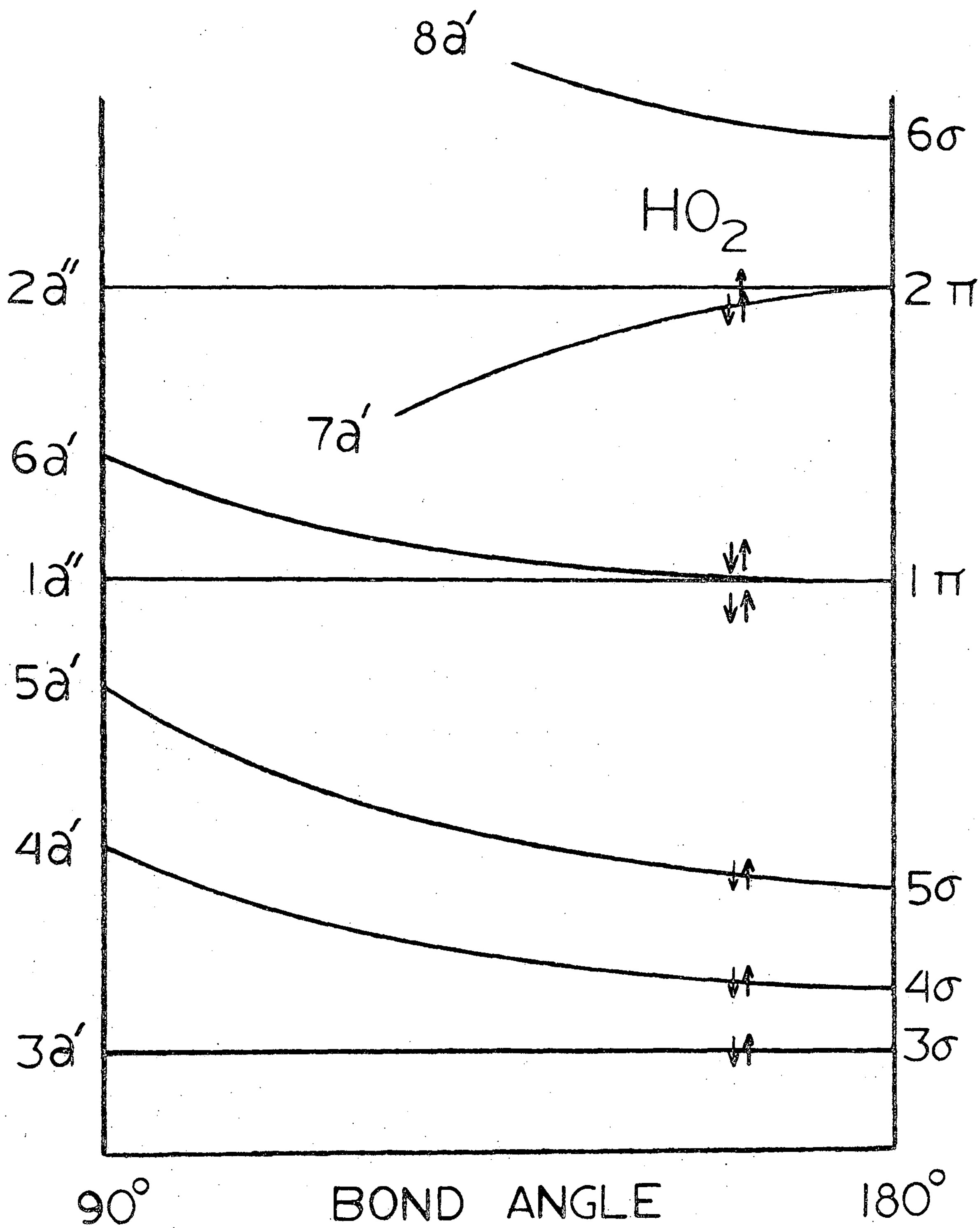

XBL 748-1414

Figure 1

B. C_3 Intramolecular Bending Potential

1. Preliminaries

Molecular carbon in the form of C_3 was known to exist in comets since the 4050 Å band was assigned to that molecule by Douglas.[1] Laboratory analysis of the 4050 Å band was accomplished[2] using flash photolysis of diazomethane by Gausset, Herzberg, Lagerqvist, and Rosen and their analysis indicated that the bending vibrational frequency, ν_2, was near 64 cm^{-1}, an unusually low value. Earlier work[3] on C_3 lead Pitzer and Clementi[4] to use the more normal value of 550 cm^{-1} for ν_2 to derive the thermodynamic functions from a calculated partition function. The entropy value, $S^o_{2500^oK}$= 77.25 eu, that they derived was in very good agreement with the experimental measurements[5,6] made from carbon vapor diffusion with the values $S^o_{2400^oK}$= 77.4 and 76.1 eu respectively. The low value reported for ν_2 means that the calculated entropy should be several entropy units higher. The contribution to the entropy due to the bending vibrational mode can be reduced if the vibration is treated as very anharmonic. In this way Strauss and Theile[7] found a theoretical lower limit entropy of $S^o_{2400^oK}$ = 79.8 eu by evaluating the classical partition function integral. Hanson and Pearson[8] also calculate $S^o_{2400^oK}$= 79.7 eu as a theoretical lower limit using a quantum mechanical model to evaluate the partition function. The remaining discrepancy of more than two entropy units forces a controversy between the accuracy of the early entropy measurements[5,6] and the low vibrational assignment of ν_2 = 64 cm^{-1}. Palmer and Shelef[9] have given a review of this problem. More entropy measurements made recently[10,11] are in accord with the theoretical and spectroscopic entropy determinations, thus supporting the low bending frequency assignment allowing that the potential is anharmonic enough to have a small entropy contribution.

This work[12] was a purely theoretical approach to investigate the bending vibrational potential with the use of ab-initio quantum mechanical electronic structure calculations on the C_3 system. In addition, a detailed description of the electronic structure is presented.

2. Basis Sets and Wavefunctions

Three somewhat different basis sets based on Huzinaga's (9s5p) gaussian basis set for the carbon atom are used in calculations on C_3. The first set is made by using Dunning's (4s2p) "Double-Zeta" contraction.[14] To improve this basis and test its accuracy, a set of d functions ($d_{xx}, d_{yy}, d_{zz}, d_{xy}, d_{xz}, d_{yz}$) is added, making the basis (4s2p1d). The added d function is a two gaussian contraction[15] approximating a 3d slater type function with 2.0 for the exponent. The SCF energies computed with the (4s2p1d) basis indicated that still more improvement is needed, so the final basis was (4s3p1d) produced by decontraction of the p function to make three independent elements. The three basis sets are presented in Table I.

All three basis sets were used to calculate SCF wavefunctions for the ground state of C_3 using C_{2v} symmetry. The ground state configuration is

$$1a_1^2\ 1b_2^2\ 2a_1^2\ 3a_1^2\ 2b_2^2\ 4a_1^2\ 3b_2^2\ 1b_1^2\ 5a_1^2 \quad ({}^1A_1)$$

written in C_{2v} symmetry. However, the C_3 molecule is known to be linear[1] in the ground state, so in $D_{\infty h}$ symmetry the ground state is

$$1\sigma_g^2\ 1\sigma_u^2\ 2\sigma_g^2\ 3\sigma_g^2\ 2\sigma_u^2\ 4\sigma_g^2\ 3\sigma_u^2\ 1\pi_u^4 \quad ({}^1\Sigma_g^+) \quad .$$

The ground state configuration can be described by a single determinant in both C_{2v} and $D_{\infty h}$ symmetries, so the nonlinear C_{2v} calculation will change smoothly to the $D_{\infty h}$ values, with the $1b_1$ and $5a_1$ orbitals becoming the $1\pi_u$ degenerate orbital.

Electron correlation in C_3 is investigated by a 656 configuration CI wavefunction calculation using the (4s2p) basis set. This CI calculation is preceeded by two other stages required to determine an orbital basis appropriate for describing correlation in the valence shell of C_3. The first stage is an ordinary single configuration SCF calculation. The second stage is a CI calculation designed to separate the higher virtual orbitals not needed for the final CI calculation. For this second stage, configurations of the type

$$1a_1^2\ 1b_2^2\ 2a_1^2\ 3a_1^2\ 2b_2^2\ 4a_1^2\ xy\ 1b_1^2\ 5a_1^2 \quad ,$$

$$1a_1^2\ 1b_2^2\ 2a_1^2\ 3a_1^2\ 2b_2^2\ 4a_1^2\ 3b_2^2\ xy\ 5a_1^2 \quad ,$$

$$1a_1^2\ 1b_2^2\ 2a_1^2\ 3a_1^2\ 2b_2^2\ 4a_1^2\ 3b_2^2\ 1b_1^2\ xy \quad ,$$

where x and y represent the unoccupied orbital basis functions $6a_1 - 14a_1$, $1a_2$, $2a_2$, $2b_1 - 4b_1$, and $4b_2$ $10b_2$. These configurations and the ground state configuration are combined for a total of 247 configurations. The final orbitals are obtained by transforming the orbitals in such a way as to diagonalize the reduced first-order density matrix.[16] This produces the natural orbitals for the 247 configuration wavefunction. The natural orbital occupation numbers for linear C_3 with R(C-C) = 2.51 bohrs are given in Table II and the $11a_1 \rightarrow 14a_1$, $2a_2$, $4b_1$, and $7b_2 \rightarrow 10b_2$ orbitals are seen to be negligible compared to the rest of the natural orbital basis set. Finally the 656 configuration CI calculation produced by taking all single and double excitations from the ground state configuration except from the carbon 1s atomic orbitals, $1a_1$, $1b_2$, and $2a_1$, is compared using the smaller basis set. This may be thought of as an extension of the Edmiston and Krauss[17] pseudonatural orbital method. In the pseudonatural orbital method, the pair excitations from the $3b_2$, $1b_1$, and $5a_1$ orbitals would be separate calculations instead of the one combined calculation used for the second stage here.

3. Bending Potential

The single configuration SCF calculations computed for each basis set as well as the CI results for the (4s2p) basis are summarized in Table III. The distance R(C-C) was optimized only for the (4s2p) CI and (4s3p1d) SCF calculations which give 2.492 bohrs and 2.404 bohrs respectively for the linear geometry. The experimental bond length[2] is 2.413 bohrs, slightly longer than the SCF result.

One surprising result is that the (4s2p1d) SCF calculation indicates C_3 to be nonlinear. The distance R(C-C) was optimized for the angles 180^o and 120^o to test the effect that the bond length has on the potential calculated in this basis, and the optimum linear energy of -113.36882 au. is still higher than the optimum energy for 120^o of -113.37013 au. The nonlinearity introduced with the addition of d functions goes away again when the p basis functions are decontracted to give the (4s3p1d) basis. A similar result has been pointed out by Stevens[18] that a 50% improvement in the ammonia inversion barrier calculated with an N(4s2p1d) basis is found with an N(4s3p1d) basis.

The inclusion of electron correlation in the C_3 wavefunction using the (4s2p) basis does not significantly change the bending potential energy, as seen in Table III. Thus, the electron correlation appears nearly constant for large changes in the bond angle, and an SCF single configuration wavefunction should be capable of accurately describing the bending potential. This also means that the most serious deficiency left in the energy is due to the limited basis set size.

The (4s3p1d) SCF bending curve is much flatter than the others and correctly predicts C_3 to be linear. Experimental evidence does not rule out a bending potential with a maximum at 180^o, however, the maximum must not exceed the first vibrational levels, as would happen for the (4s2p1d) case.

The calculated potential energy functions for the (4s2p) CI and (4s3p1d) SCF wavefunctions are smoothed with a cubic spline fit and used to calculate bending vibrational energy levels. In considering the bending mode, ν_2, for an AB_2 or A_3, triatomic molecule the vibrational Hamiltonian can be simplified by requiring that the bond length be a constant. The two dimensional Hamiltonian then becomes one dimensional in the angle of the molecule. The reduced masses for the AB_2 molecule are found in the two dimensional cartesian coordinate Hamiltonian which takes the quantum mechanical form

$$H = -\frac{1}{2}\left[\frac{2M_B + M_A}{2M_BM_A}\frac{\partial^2}{\partial y^2} + \frac{1}{2M_B}\frac{\partial^2}{\partial x^2}\right] + V(x,y) \qquad (4)$$

$$\mu_y = \frac{2M_BM_A}{2M_B+M_A} \qquad \mu_x = 2M_B$$

where the coordinates are defined in Figure 1. Upon substitution of the generalized coordinated R and θ, this cartesian coordinate Hamiltonian changes into the following form

$$H = -\frac{1}{2}\left[\frac{1}{R}\frac{\partial}{\partial R} R\left(\frac{\sin^2\theta}{\mu_y} + \frac{\cos^2\theta}{\mu_x}\right)\frac{\partial}{\partial R} + \frac{1}{R}\frac{\partial}{\partial R}\left(\frac{1}{\mu_y} - \frac{1}{\mu_x}\right)\sin\theta\cos\theta\frac{\partial}{\partial\theta} + \right.$$

$$\left.\frac{1}{R}\frac{\partial}{\partial\theta}\left(\frac{1}{\mu_y} - \frac{1}{\mu_x}\right)\sin\theta\cos\theta\frac{\partial}{\partial R} + \frac{1}{R^2}\frac{\partial}{\partial\theta}\left(\frac{\cos^2\theta}{\mu_y} + \frac{\sin^2\theta}{\mu_x}\right)\frac{\partial}{\partial\theta}\right] + V(R,\theta).$$

(5)

The one dimensional Hamiltonian for the θ coordinate results when the terms in Eq. (5) involving $\frac{\partial}{\partial R}$ are dropped and R is fixed. For A and B atoms the same, the final form for the bending Hamiltonian is reduced to the form

$$H = -\frac{\partial}{\partial\theta} \frac{2\cos^2\theta + 1}{4m} \frac{\partial}{\partial\theta} + V(R,\theta)$$

where m is the mass of one carbon atom of C_3. This formula is used in a computer program to solve the one dimensional differential equation numerically. The resulting eigenvalues are listed in Table IV, along with the level separations. The separations calculated for the (4s2p) CI potential indicate a steeper more harmonic potential than for the (4s3p1d) SCF potential, which is shown in Figure 2. This potential is obviously very anharmonic, and the unusual "dimple" found in the middle of the potential is responsible for the uneven spacings found between the initial vibrational levels. This analysis is not rigorous since the stretching vibrations in the R coordinate cannot be trivialy decoupled from bending as assumed here by fixing R. However, this analysis does indicate that C_3 does indeed have a smaller than usual $\nu_2 = 64\ cm^{-1}$ measured by Gausset et al.[2]

4. Analysis

A Walsh-like diagram can be made by using the occupied SCF orbital energies for C_3. Walsh[19] originally estimated general trends expected for orbital energies of deformed molecules based on correlation diagrams for hybridized atomic orbitals. However, the (4s3p1d) SCF orbital energies listed in Table V can be used to make a Walsh diagram specific for C_3, as seen in Figure 3. This illustration shows that the valence orbitals $5a_1$, $1b_1$, and $3b_2$ contribute no significant restoring force until the bond angle has reached nearly 100°, where the $3b_2$ orbital begins to rise above the others. The lowest unoccupied orbital for C_3, the $1\pi_g$, is expected to have a much larger restoring force as shown in calculations on O_3 and N_3^- made by Peyerimhoff and Buenker,[20] and predicted by Walsh.[19]

The $2b_2$ and $4a_1$ orbitals in the 60° bond angle calculation do not become degenerate as required by symmetry because the single determinant wavefunction sufficient for C_{2v} geometry does not describe a pure symmetry state in D_{3h} geometry. In D_{3h} symmetry the ground state configuration is

$$1a_1'^2\ 1e'^4\ 2a_1'^2\ 2e'^4\ 1a_2''^2\ 3a_1'^2\ 3e'^2 \quad ({}^1E') \tag{7}$$

which is constructed by a minimum of two determinants

$$\Psi({}^1E') = \frac{1}{\sqrt{2}} (3e_x'\ \alpha\ 3e_x'\ \beta - 3e_y'\ \alpha\ 3e_y'\ \beta) \tag{8}$$

or in C_{2v} symmetry

$$\Psi({}^1A_1) = \frac{1}{\sqrt{2}} (3b_2\ \alpha\ 3b_2\ \beta - 6a_1\ \alpha\ 6a_1\ \beta) \quad . \tag{9}$$

The single determinant calculation results in a mixture of ${}^1A_1'$ and ${}^1E'$ states at 60° and fails to make the required orbitals degenerate. An

SCF calculation using the (4s2p) basis and the two configuration wavefunction, Eq. (9), yields an energy of -113.1851 Hartrees compared to -113.1721 for the single configuration with the same basis at 60°. The second determinant needed for the D_{3h} symmetry should combine smoothly in the CI calculation, but in the linear geometry it has a small coefficient of 0.0103. Table VI shows the most important configurations in the linear C_3 wavefunction near the equilibrium geometry.

1. A. E. Douglas, Astrophys, J. 114, 466 (1951).

2. L. Gausett, G. Herzberg, A. Lagerqvist, and B. Rosen, Astrophys. J. 142, 45 (1965), Discussions Farad. Soc. 35, 113 (1963).

3. N. H. Keiss and H. P. Broida, Can. J. Phys. 34, 1971 (1956).

4. K. S. Pitzer and E. Clementi, J. Am. Soc. 81, 4477 (1959).

5. R. J. Thorn and G. H. Winslow, J. Chem. Phys. 26, 186 (1957).

6. J. Drowert, R. P. Burns, G. Demarie, and M. G. Ingram, J. Chem. Phys. 31, 1131 (1959).

7. H. L. Strauss and E. Thiele, J. Chem. Phys. 46, 2473 (1967).

8. C. F. Hansen and W. E. Pearson, Can. J. Phys. 51, 751 (1973).

9. H. B. Palmer and M. Shelef, "Vaporization of Carbon," Chemistry and Physics of Carbon, Vol. IV, Marcel Dekker Inc., New York 1968, pp. 85-135.

10. P. D. Zavitsanos, "Experimental Study of the Sublimination of Graphite at High Temperature," General Electric Re-entry and Environmental System Division, Philadelphia, Pa. 01901, (unpublished report).

11. F. M. Wachi and D. F. Gilmartin, 20th Annual Conference on Mass Spectrometry and Applied Topics, June 4-9, 1972, Dallas, Texas, paper D4.

12. D. H. Liskow, C. F. Bender, and H. F. Schaefer, III, J. Chem. Phys. 56, 5075 (1972).

13. S. Huzinaga, J. Chem. Phys. 42, 1293 (1965).

14. T. H. Dunning, J. Chem. Phys. 53, 2823 (1970).

15. T. H. Dunning, J. Chem. Phys. 55, 3958 (1971).

16. R. McWeeny and B. T. Sutcliffe, Methods of Molecular Quantum Mechanics,

Academic Press, London, 1969.

17. C. Edmiston and M. Krauss, J. Chem. Phys. 45, 1833 (1966).

18. R. M. Stevens, J. Chem. Phys. 55, 1725 (1971).

19. A. D. Walsh, J. Chem. Soc. (1953) 2260, and following five papers.

20. S. D. Peyerimhoff and R. J. Buenker, J. Chem. Phys. 47, 1953 (1967).

Table I. Gaussian Basis Sets Used for C_3 Calculations.

Primitive Gaussian Exponents		Basis I	Basis II	Basis III
		------ contraction coefficients -----		
(9s5p)[a]	(2d)[b]	(4s2p)[c]	(4s2p1d)	(4s3p1d)
s	4232.61	0.002029	Same	Same
	634.882	0.015535		
	146.097	0.075411		
	42.4974	0.257121		
	14.1892	0.596555		
	1.9666	0.242517		
	5.1477	1.0	1.0	1.0
	0.4962	1.0	1.0	1.0
	0.1533	1.0	1.0	1.0
p	18.1557	0.018534	Same	0.039196
	3.9864	0.115442		0.244144
	1.1429	0.386206		0.816775
	0.3594	0.640089		1.0
	0.1146	1.0	1.0	1.0
d	1.3089	---	0.357851	Same
	0.3877	---	0.759561	

[a]Ref. 13

[b]Ref. 15

[c]Ref. 14

TABLE II. Natural orbital occupation numbers for the 247-configuration wavefunction. The bond angle was 180° and the C–C bond distance 2.51 bohr.

$1a_1$	2.0	$1a_2$	0.04447	$1b_1$	1.94480	$1b_2$	2.0
$2a_1$	2.0	$2a_2$	0.00003	$2b_1$	0.01384	$2b_2$	2.0
$3a_1$	2.0			$3b_1$	0.00056	$3b_2$	1.98650
$4a_1$	2.0			$4b_1$	0.00004	$4b_2$	0.04446
$5a_1$	1.94481					$5b_2$	0.00122
$6a_1$	0.01384					$6b_2$	0.00051
$7a_1$	0.00275					$7b_2$	0.00004
$8a_1$	0.00116					$8b_2$	0.00003
$9a_1$	0.00112					$9b_2$	0.00001
$10a_1$	0.00056					$10b_2$	0.00000
$11a_1$	0.00037						
$12a_1$	0.00004						
$13a_1$	0.00001						
$14a_1$	0.00000						

XBL 748-1415

TABLE III. Summary of calculated C_3 electronic energies as a function of bond angle. In the second and fourth series of calculations, the total energy was minimized with respect to bond distance for each bond angle. The experimental bond distance is 2.413 bohrs.[a]

θ	R(bohr)	E(hartree)
	(4s2p) basis, SCF	
180°	2.4	−113.32135
160°	2.4	−113.31817
140°	2.4	−113.30955
120°	2.4	−113.29718
100°	2.4	−113.27989
	(4s2p) basis, 656 configurations	
180°	2.492	−113.52215
160°	2.493	−113.51932
140°	2.504	−113.51277
120°	2.511	−113.50561
60°	2.724	−113.40815
	(4s2p1d) basis, SCF	
180°	2.41	−113.36851
160°	2.41	−113.36862
140°	2.41	−113.36912
120°	2.41	−113.36979
100°	2.41	−113.36776
80°	2.41	−113.35020
	(4s3p1d) basis, SCF	
180°	2.404	−113.380851
160°	2.404	−113.380577
140°	2.405	−113.380358
120°	2.409	−113.380286
110°	2.412	−113.379695
100°	2.418	−113.377748

[a] Reference 2

XBL 748-1416

TABLE IV. Vibrational energy levels in cm^{-1} for the bending of C_3. ΔE indicates the spacing between adjacent vibration levels.

	(4s2p) CI E_n	ΔE		(4s3p1d) SCF E_n	ΔE
0	161	...	0	47	...
1	478	317	1	116	69
2	783	305	2	155	38
3	1080	297	3	199	44
4	1369	289	4	257	58
5	1649	280	5	325	68
			6	401	76
			7	484	83
			8	574	90
			9	672	98
			10	781	108
			11	900	119
			12	1028	128
			13	1164	136
			14	1307	143
			15	1456	150

XBL 748-1417

Table V. Total and orbital energies (in hartrees) for C_3 as a function of bond angle. The C–C bond distance in all calculations was 2.41 bohr. The C(4*s*3*p*1*d*) basis set was used.

	60°	80°	100°	120°	140°	160°	180°
E(total)	−113.26216	−113.36055	−113.37770	−113.38028	−113.38034	−113.38055	−113.38082
$1a_1$	−11.3316	−11.3535	−11.3641	−11.3689	−11.3714	−11.3728	−11.3734
$2a_1$	−11.3276	−11.2947	−11.2648	−11.2493	−11.2428	−11.2404	−11.2398
$1b_2$	−11.3269	−11.3531	−11.3639	−11.3688	−11.3713	−11.3728	−11.3733
$3a_1$	−1.3658	−1.2706	−1.2046	−1.1641	−1.1409	−1.1289	−1.1253
$2b_2$	−0.7256	−0.7966	−0.8563	−0.9016	−0.9329	−0.9515	−0.9576
$4a_1$	−0.7098	−0.6168	−0.5697	−0.5500	−0.5429	−0.5406	−0.5401
$1b_1$	−0.5817	−0.5324	−0.5030	−0.4870	−0.4793	−0.4760	−0.4752
$5a_1$	−0.5188	−0.5035	−0.4930	−0.4851	−0.4794	−0.4762	−0.4752
$3b_2$	−0.3811	−0.4525	−0.4832	−0.4958	−0.5016	−0.5042	−0.5050

XBL 748-1418

LBL-2980

TABLE VI. Most important configurations for C_3, $\theta = 180°$, R(C–C) = 2.51 bohr.

Spatial configuration	Coefficient	Energy criterion
(1) $1a_1^2 1b_2^2 2a_1^2 3a_1^2 2b_2^2 4a_1^2 3b_2^2 5a_1^2 1b_1^2$	0.94745	...
(2) $5a_1 1b_1 \rightarrow 1a_2 4b_2$	0.10942	−0.00902
(3) $5a_1 1b_1 \rightarrow 6a_1 2b_1$	0.06849	−0.00584
(4) $5a_1^2 \rightarrow 6a_1^2$	0.05573	−0.00348
(5) $1b_1^2 \rightarrow 2b_1^2$	0.05573	−0.00348
(6) $1b_1^2 \rightarrow 1a_2^2$	0.07444	−0.00327
(7) $5a_1^2 \rightarrow 4b_2^2$	0.07444	−0.00327
(8) $4a_1 3b_2 \rightarrow 7a_1 5b_2$	0.03554	−0.00277

XBL 748-1419

FIGURE CAPTIONS

Figure 1. Coordinate system for bending an AB_2 symmetric molecule.

Figure 2. Bending potential energy for C_3 calculated with the (4s3p1d) SCF wavefunction. The C-C bond length is optimized at each angle on the curve.

Figure 3. Orbital energies of C_3 as a function of bond angle. The C-C bond distance is 2.41 bohrs at all angles.

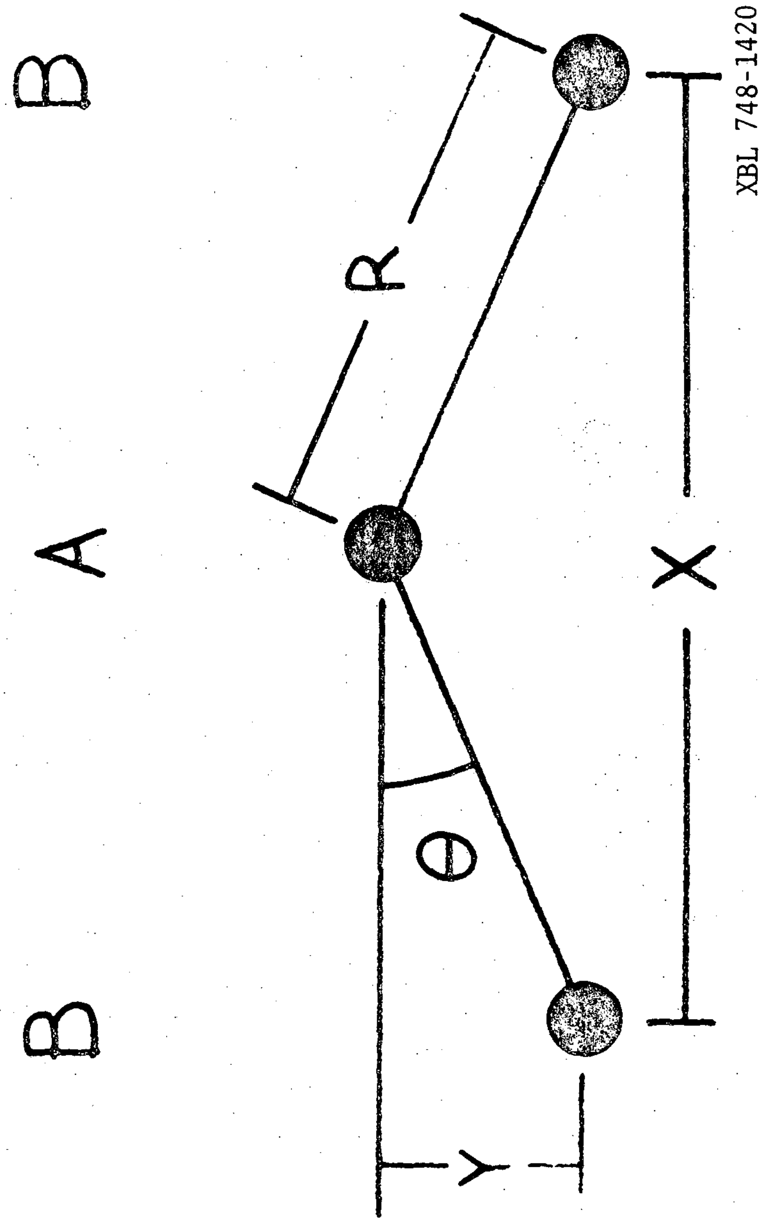

Figure 1

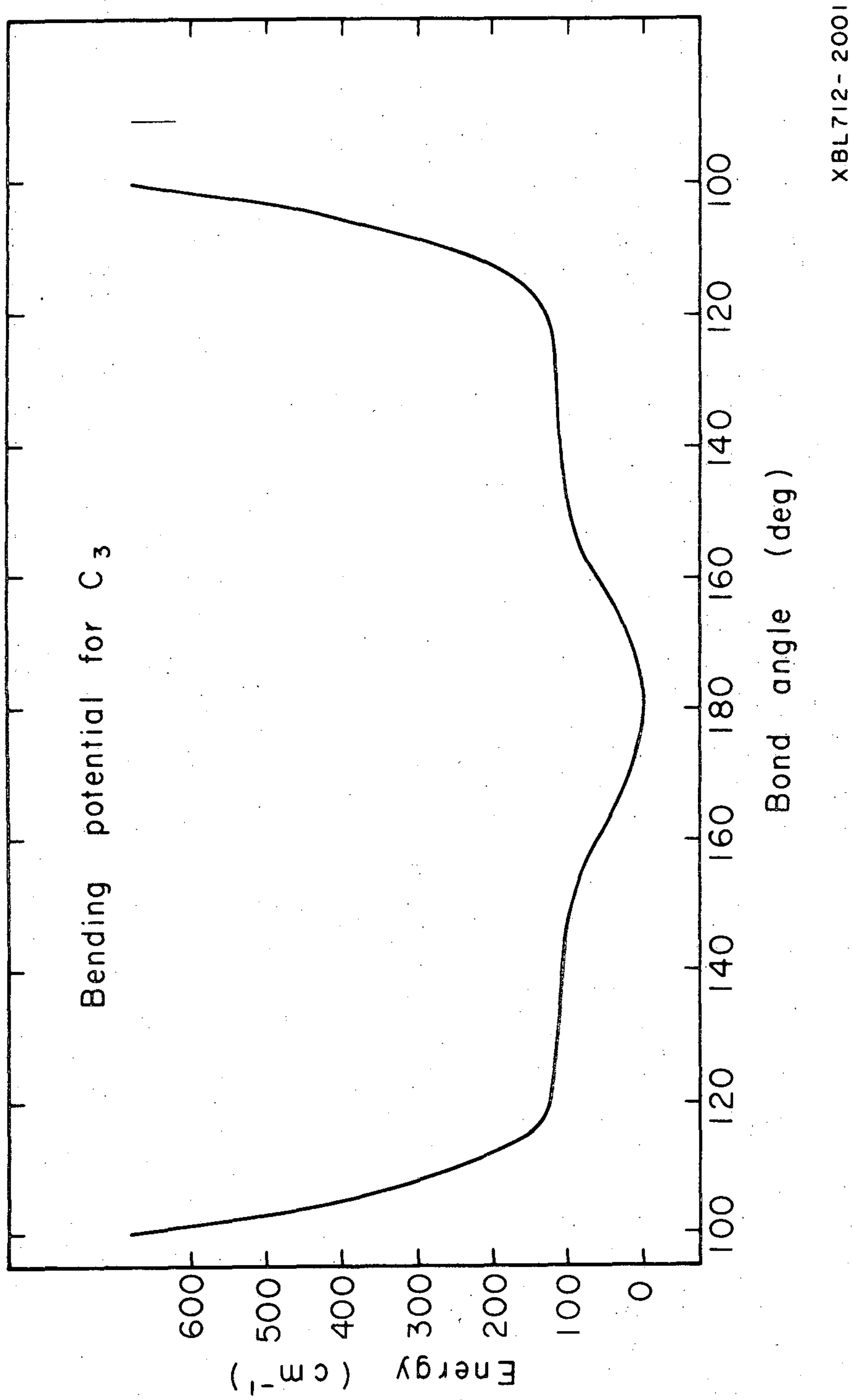
Bending potential for C_3
Energy (cm^{-1})
600
500
400
300
200
100
0
Bond angle (deg)
100
120
140
160
180
160
140
120
100
XBL712-2001

Figure 2

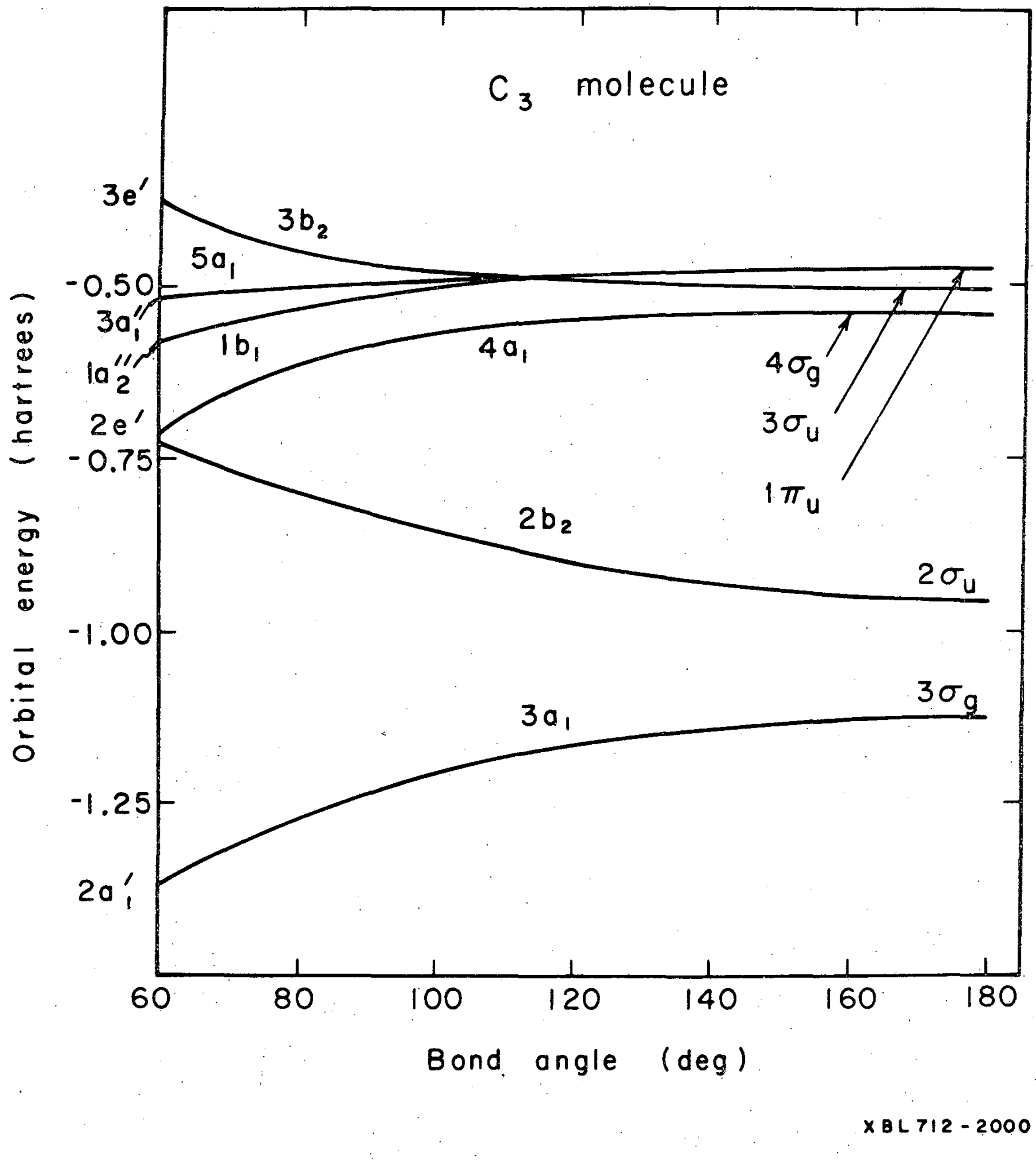
C 3 molecule
3e′
3b2
5a1
-0.50
3a1″
1b1
1a2″
4a1
4σg
3σu
2e′
-0.75
1πu
2b2
2σu
-1.00
3σg
3a1
-1.25
2a1′
60
80
100
120
140
160
180
Bond angle (deg)
Orbital energy (hartrees)
XBL 712-2000

Figure 3

C. $CH_3NC \rightarrow CH_3CN$ A Unimolecular Isomerization

1. Preliminaries

The $CH_3NC \rightarrow CH_3CN$ reaction is a well known thermal unimolecular isomerization. The kinetics of this reaction have been studied experimentally by Rabinovitch and coworkers[1] for several years, providing a wealth of information with which to compare theoretical investigations of the isomerization reaction. Several theoretical electronic structure calculations dealing with the methyl isocyanide isomerization transition have been made[2-4] but these calculataions each involve at least one severe approximation that invites continued effort on this reaction. This work[5] is a new step toward an accurate potential energy surface based on *ab-initio* electronic structure calculations. The object of the present work is to characterize the qualitative features of the potential energy surface such as the saddle point for the isomerization and the minimum energy reaction path.

2. Basis Set and Wavefunction

The basis set used is the usual "double zeta" basis formed with Huzinaga's[6] (9s5p) gaussian basis for carbon and nitrogen, and the (4s) set for hydrogen, by using Dunning's[7] contraction scheme. The contraction produces a (4s2p) basis for both carbons and the nitrogen atom, and a (2s) set for each hydrogen atom, making a total of 36 contracted Gaussian functions. Based on previous experience,[8] the quality of this basis set in conjunction with a single configuration SCF wavefunction should be good enough for obtaining reliable molecular geometries.

The isomerization of CH_3NC to form CH_3CN can be minimally described with a single configuration wavefunction. The reactant and product molecules both have the same closed shell orbital occupancy, and should have nearly the same electron correlation error when described by a single configuration. However, the intermediate conformations along the reaction path should have a significantly greater correlation error resulting from the use of a single configuration wavefunction. Thus, the predicted barrier height may be too high, but the qualitative features of the surface will remain because the ground state configuration is the same for both the reactant and the product molecules.

3. Geometry Optimization and Reaction Path

There are $3 \cdot 6 - 6 = 12$ internal coordinates required to uniquely characterize the conformation of the six atoms in the CH_3NC system. To minimize computational effort, the number of coordinates is reduced by requiring the molecule to retain certain standard coordinates not directly involved in the isomerization. The coordinates basic to the isomerization are diagrammed in Figure 1, where R is the distance from the methyl carbon to the CN center of mass, and θ is the polar angle for rotation of the CN bond around its center of mass which is located on the C_3 symmetry axis of the methyl group. The angle θ is 0^{o} for CH_3CN and is 180^{o} for CH_3NC. This standardized geometry also requires the CH_3 group to have C_{3v} local symmetry, a CH bond distance of 1.10 Å, a CN bond distance of 1.16 Å, the HCX angle to be 110^{o} (X is the CN center of mass), and the carbon atom in the CN group eclipsing a CH_3 hydrogen atom in the conformations with non-linear CCN. Experimentally[9] the CH bond length is 1.103 Å in CH_3CN and 1.101 Å in CH_3NC, and the HCX angle is 109^{o} 30' in CH_3CN and 109^{o} 7' in CH_3NC. Finally, a coordinate ϕ is used to measure the CH_3 rotation with respect to the CN group around the C_3 symmetry axis in the transitional conformations. By definition $\phi = 0^{o}$ for N eclipsed and $\phi = 60^{o}$ for C eclipsed.

The reaction profile is calculated for standard geometry and optimum R for each $\theta = 0^{o}$, 45^{o}, 90^{o}, 135^{o}, and 180^{o}, except at 90^{o} where the CN distance and the HCX angle were also optimized. The geometry optimization for $\theta = 90^{o}$ was performed in cycles by optimizing one coordinate at a time in the order R, R(CN), and HCX angle. The reaction profile created this way is shown in Table I. The second calculation at 90^{o} for $\phi = 0^{o}$ uses the geometry optimized for $\phi = 60^{o}$ (C atom eclipsed).

The activation energy for a reaction can be compared to the energy needed to reach the saddle point energy from the reactant ground state. The saddle point is the top of the lowest energy path leading to the product of the reaction, and for CH_3NC the saddle point is found for $\theta = 100.8^o$ as shown in Table II. Table II is the result of further geometry optimization for the reactant CH_3NC, and product CH_3CN, and the saddle point conformations. This table indicates a reaction exothermicity of 17.3 kcal/mole and a barrier for the reaction of 60.4 kcal/mole. As expected the barrier is higher than the experimental activation energy[1a] of 38.4 kcal/mole, however, the exothermicity is very close to estimates[3,10] based on heats of formation ranging from 14.7 to 16.8 kcal/mole. More significant is the predicted geometry of the saddle point. The transition state geometry predicted by Van Dine and Hoffman[2] using extended Hückel calculations has a planar CH_3 group and is very ionic, $[CH_3^{+.59}]$ $[CN^{-.59}]$, while Dewar and Kohn[3] using MINDO/2 and Moffat and Tang[4] using CNDO/2 find a metastable intermediate (local minimum) near the saddle point. To check for the metastable intermediate discovered using semiempirical methods, Table III shows a more detailed reaction profile near the calculated saddle point. Since the geometry is optimized for only the saddle point, this table indicates that there is no metastable intermediate, and that the observation of one appears to be an artifact of the semiempirical methods used to discover it. By forcing the CH_3 group to be planar near the transition with $\theta = 90^o$, the energy with optimum R and R(CN) is raised by 14.1 kcal/mole. This means the CH_3

remains pyramidal at the saddle point contrary to extended Hückel prediction.

A more detailed look at the potential energy surface along the reaction path is provided in Table IV. This table shows the internal barrier to rotation of the CH_3 group around its C_3 axis for $\theta = 45^o$, 90^o, and 135^o. The change in sign of the barrier for $\theta = 135^o$ can be explained by steric arguments since the N atom is closer to the H_3 plane for $\theta = 135^o$ and the C atom is closer for $\theta = 45^o$. Harris and Bunker[11] predicted that CH_3NC was a non-RRKM molecule, but further consideration of rotational effects,[12] and the internal rotation in particular, weakens their initial prediction.

4. Electron Distribution and Observable Properties

Casanova, Werner, and Schuster[13] describe the isomerization reaction as a synchronous process going smoothly from the reactant to the transition state and to the product molecules. These calculations support that description in that the transition state geometry remains pyramidal and does not alter significantly from the starting methyl geometry. Another way to look at this is with the Mulliken population analysis[14] for the wavefunction during the rearrangement. This kind of analysis, albeit arbitrary, allows comparison with other calculations like that of Van Dine and Hoffman.[2] Populations are given in Table V and comparison shows that the planar transition state is very ionic, in agreement with Van Dine and Hoffman. However, at a lower energy the non-planar CH_3 transition state populations are between the methyl populations for CH_3NC and CH_3CN. Again a synchronous change is indicated by the smooth change in CH_3 charge presented with Mulliken population analysis.

A more useful approach to indicate atomic charges is to look at the electric potential at the nuclei and the inner shell ionization potentials. These observable properties can be correlated to the concept of an atomic charge.[15-17] The potential calculated at the CH_3NC nuclei during the isomerization are also presented in Table V, and the SCF orbital energies which correspond to calculated ionization energies in the sense of Koopmann's theorem are given in Table VI. The electric potential at a nucleus shows a shift to lower values when the charge becomes more negative at that atom, and the inner shell ionization decreases when the atomic charge is more negative. The trends for both of these properties agree in each case during the isomerization. However, there is some disagreement with the Mulliken population at the transition state, where the methyl carbon becomes more positive than for either CH_3NC or CH_3CN, but not as positive as it would be in the planar methyl transition state.

Finally, Table VII shows the effect of the isomerization reaction on several other molecular properties. Previous experience[18] indicates that larger than double zeta basis sets are needed to guarantee accurate dipole moments, but the highly polar nature of the CH_3NC and CH_3CN molecules makes the good agreement not so surprising.

5. Conclusion

Investigation of the isomerization of CH_3NC by using *ab-initio* SCF calculations has shown the transition state geometry to have a nonplanar CH_3 structure at a saddle point with $\theta = 100.8^0$ and an energy 60.4 kcal/mole above the reactant molecule, CH_3NC. The experimental activation energy[1a] of 38.4 kcal/mole is significantly lower than the calculated saddle point energy because electron correlation effects are neglected in the SCF wavefunction.[18,19] However, the other features of the surface can be calculated with a minimum amount of effort, using a single determinant wavefunction which neglects correlation. Features specifically investigated are the geometry of the transition state and the barrier to internal rotation of the methyl group during isomerization.

REFERENCES

1a. F. W. Schneider and B. S. Rabinovitch, J. Am. Chem. Soc. 84, 4215 (1962).

1b. F. W. Schneider and B. S. Rabinovitch, J. Am. Chem. Soc. 85, 2365 (1963).

1c. B. S. Rabinovitch, P. W. Gilderson, and F. W. Schneider, J. Am. Chem. Soc. 87, 158 (1965).

1d. S. C. Chan, B. S. Rabinovitch, J. T. Bryant, L. D. Spicer, T. Fujimoto, Y. N. Lin, and S. P. Pavlou, J. Phys. Chem. 74, 3160 (1970).

2. G. W. Van Dine and R. Hoffman, J. Am. Chem. Soc. 90, 3227 (1968).

3. M. J. S. Dewar and M. C. Kohn, J. Am. Chem. Soc. 94, 2705 (1972).

4. J. B. Moffat and K. F. Tang, Theor. Chim. Acta. 32, 171 (1973).

5a. D. H. Liskow, C. F. Bender, and H. F. Schaefer, III. J. Am. Chem. Soc. 94, 5178 (1972).

5b. D. H. Liskow, C. F. Bender, and H. F. Schaefer, III, J. Phys. Chem. 57, 4509 (1972).

6. S. Huzinaga, J. Phys. Chem. 42, 1293 (1965).

7. T. H. Dunning, J. Chem. Phys. 53, 2823 (1970).

8. L. Radom, W. J. Here, and J. A. Pople, J. Am. Chem. Soc. 94, 2371 (1972).

9. C. C. Costain, J. Chem. Phys. 29 864 (1958).

10. S. W. Benson, J. Chem. Educ. 42, 502 (1965).

11. H. H. Harris and D. L. Bunker, Chem. Phys. Letters 11, 433 (1971).

12. D. L. Bunker, J. Chem. Phys. 57, 332 (1972).

13. J. Casanova, N. D. Werner, and R. E. Schuster, J. Org. Chem. 31, 3473 (1966).

14. R. S. Mulliken, J. Chem. Phys. 23, 1833 (1955).

15. K. Siegbahn, C. Nordling, G. Johansson, J. Hedman, P. F. Heden, K. Hemrin, U. Gelius, T. Bergmark, L. O. Werme, R. Manne, and Y. Baer, ESCA Applied to Free Molecules, North-Holland Publishing Co., Amsterdam, 1969.

16. M. E. Schwartz, Chem. Phys. Letters 6, 631 (1970).

17. H. Basch, Chem. Phys. Letters 5, 337 (1970).

18. H. F. Schaefer, III, The Electronic Structure of Atoms and Molecules: A Survey of Rigorous Quantum Mechanical Results, Addison-Wesley, Reading, Massachusetts, 1972.

19. C. F. Bender, P. K. Pearson, S. V. O'Neil, and H. F. Schaefer, III, Science 176, 1412 (1972), J. Chem. Phys. 56, 4626 (1972).

Table I. Summary of Self-Consistent-Field Energies for the Methyl Isocyanide Rearrangement[a]

Description	θ, deg	R	Other geometrical parameters	E, hartrees	E, kcal
CH_3NC	180	1.971	Standard	−131.8507	0.0
	135	1.864	Standard	−131.8034	29.7
$\phi = 0°$	90	1.802	$R(CN) = 1.203$, $\theta(HCX) = 106°$	−131.7570	58.8
$\phi = 60°$	90	1.802	$R(CN) = 1.203$, $\theta(HCX) = 106°$	−131.7557	59.6
Planar CH_3	90	2.013	$R(CN) = 1.2$, $\theta(HCX) = 90°$	−131.7346	72.9
	45	1.990	Standard	−131.7979	33.1
CH_3CN	0	2.097	Standard	−131.8785	−17.4

[a] Distances are given in Ångströms; θ and R are defined in Figure 1.

XBL 748-1421

LBL-2980

Table II. Geometries and energies of three points on the minimum energy path for $CH_3NC \rightarrow CH_3CN$. Unless indicated experimental values, given in parentheses, are from C. C. Costain, J. Chem. Phys. **29**, 864 (1958).

Parameter	CH_3NC	Saddle point	CH_3CN
θ	180° (180°)	100.8°	0° (0°)
ϕ	...	0°	...
HCX Angle	110.0° (109.1)	106.2°	110.0° (109.5°)
R(CH)	1.081 Å (1.101)	1.074 Å	1.082 Å (1.102)
R(CX)	1.967 Å (1.962)	1.822 Å	2.086 Å (2.081)
R(CN)	1.167 Å (1.166)	1.198 Å	1.146 Å (1.157)
E (hartrees)	−131.85166	−131.75546	−131.87927
E (kcal/mole)	0.0	60.4 (38.4[a])	−17.3 (between −14.7 and −16.8)[b]

[a] Experimental activation energy of Ref. 1a

[b] See heat of formation data given in Ref. 3

XBL 748-1422

LBL-2980

TABLE III. Some points near the saddle point on the $CH_3NC \rightarrow CH_3CN$ potential surface. All geometrical parameters except θ (see Fig. 1) are those predicted for the saddle point (middle column, Table II).

θ	E (hartrees)	E (kcal/mole)
130.8	−131.77609	47.42
120.8	−131.76518	54.27
110.8	−131.75971	57.70
105.8	−131.75593	60.07
100.8	−131.75546	60.37
95.8	−131.75614	59.94
90.8	−131.75782	58.88
80.8	−131.76353	55.30
70.8	−131.77171	50.17
60.8	−131.78183	43.82

XBL 748-1423

Table IV. Methyl rotational barrier accompanying the isocyanide isomerization. θ is defined by Fig. 1, and ϕ in the text. The energy in hartrees is given above the relative energy in kilocalories per mole.

	θ		
ϕ	135°	90°	45°
0°	−131.80106 1.48	−131.75698 0.00	−131.80074 0.00
20°	−131.80167 1.10	−131.75664 0.21	−131.79999 0.47
40°	−131.80284 0.36	−131.75599 0.62	−131.79847 1.42
60°	−131.80342 0.00	−131.75568 0.82	−131.79770 1.91

XBL 748-1424

Table V. Population Analyses and Potential Calculated at Each Nucleus in CH_3CN

	CH_3NC	$\theta = 90°$ $\theta(HCX) = 106°$	Planar $\theta(HCX) = 90°$	CH_3CN
		Atomic Charges		
H	0.22	0.26	0.28	0.23
C_{methyl}	−0.41	−0.52	−0.43	−0.58
N	−0.20	−0.21	−0.28	−0.10
C	−0.07	−0.01	−0.12	−0.02
		Potentials		
H	−1.062	−1.032	−0.999	−1.048
C_{methyl}	−14.6463	−14.6277	−14.6071	−14.6661
N	−18.3329	−18.3274	−18.3526	−18.3408
C	−14.6965	−14.6913	−14.7163	−14.6783

XBL 748-1425

Table VI. Orbital Energies (in Hartrees) for Four CH_3CN Geometries

		θ = 90°		
	CH_3NC	Lowest energy θ(HCX) = 106°	Planar θ(HCX) = 90°	CH_3CN
E(total)	−131.8507	−131.7570	−131.7346	−131.8785
1a′	−15.5993	−15.6235	−15.5963	−15.6035
2a′	−11.3136	−11.3371	−11.3675	−11.3061
3a′	−11.3006	−11.3102	−11.2835	−11.2946
4a′	−1.2874	−1.2937	−1.2551	−1.2517
5a′	−1.0341	−0.9772	−0.9927	−1.0400
6a′	−0.7376	−0.6899	−0.6900	−0.6948
7a′	−0.6414	−0.5737	−0.5819	−0.6281
8a′	−0.4780	−0.5336	−0.4780	−0.5517
9a′	−0.4643	−0.4610	−0.4426	−0.4682
1a″	−0.6414	−0.6413	−0.6689	−0.6281
2a″	−0.4780	−0.4814	−0.4649	−0.4682

XBL 748-1426

TABLE VII. Some Molecular Properties (in Atomic Units) for CH_3CN[a]

	CH_3NC	Saddle point $\theta(HCX) = 106°$	Saddle point $\theta(HCX) = 90°$	CH_3CN
		Dipole Moment		
μ_y	−1.46 (−1.51 ± 0.02[b])	−1.135	−1.76	−1.66 (−1.54 ± 0.02[b])
μ_z	0.0	−0.013	−0.009	0.0
		Quadrupole Moment Tensor		
θ_{xx}	1.19	0.92	1.31	1.12
θ_{yy}	−2.39 (−2.0 ± 1.2[c])	2.34	1.89	−2.24 (−1.3 ± 0.9[c])
θ_{zz}	1.19	−3.25	−3.21	1.12
θ_{yz}	0.00	0.01	−0.01	0.00
		Second Moments of the Electron Distribution		
$\langle x^2 \rangle$	−19.05 (−19 ± 2[c])	−19.52	−19.82	−19.05 (−19 ± 1[c])
$\langle y^2 \rangle$	−116.64 (−116 ± 2[c])	−82.75	−90.49	−126.91 (−124 ± 1[c])
$\langle z^2 \rangle$	−19.05 (−19 ± 2[c])	−39.00	−39.45	−19.05 (−19 ± 1[c])
$\langle yz \rangle$	0.00	−0.02	−0.02	0.00
		Electric Field Gradient Tensor at Methyl Carbon		
q_{xx}	0.23	0.32	0.46	0.14
q_{yy}	−0.46	−0.66	−0.94	−0.28
q_{zz}	0.23	0.34	0.48	0.14
q_{yz}	0.00	−0.03	−0.03	0.00

[a] For CH_3NC and CH_3CN at equilibrium, the *y* axis contains the CN group. At the saddle point the *z* axis includes the CN group. Experimental values are in parentheses. [b] S. N. Ghosh, R. Trambarulo, and W. Cordy, *J. Chem. Phys.*, **21**, 308 (1953). [c] J. M. Pochan, R. L. Schoemaker, R. G. Stone, and W. H. Flygare, *J. Chem. Phys.*, **52**, 2478 (1970).

XBL 748-1427

FIGURE CAPTION

Figure 1. Coordinate system for treating CH_3NC isomerization to CH_3CN. The CN group turns on its center of mass which is located on the CH_3 group C_3 axis.

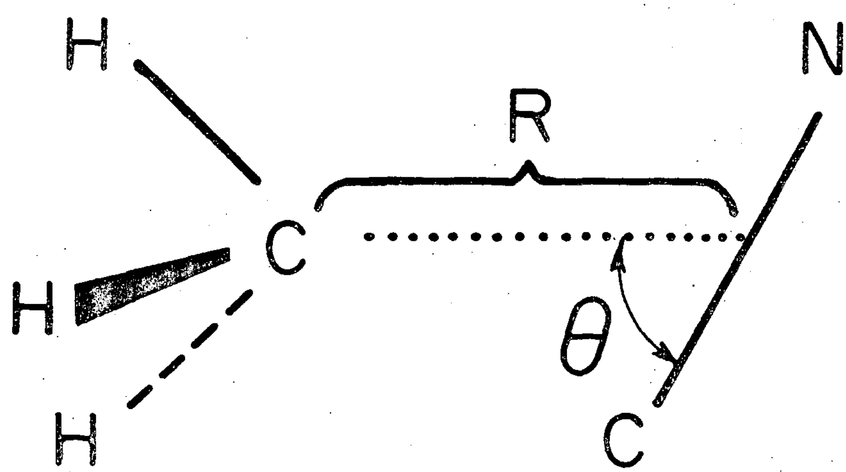

XBL727-3556

Figure 1

D. $C^+ + H_2 \rightarrow CH_2^+ \rightarrow CH^+ + H$ An Ion-Molecule Reaction

1. Preliminaries

The C^+ and H_2 reaction has been under experimental investigation for several years now, and recent evidence has begun serious discussions of the reaction mechanism. The first experiments by Maier[1] consisted of tandem mass spectrometer detection of CH^+ and determined the threshold energy to be 0.4 eV from the total cross section. Subsequently Iden, Liardon, and Koski[2,3] made more detailed experiments which measured reaction product velocity distributions, and indicated nearly isotropic product scattering at low relative energies (3.5 eV), and forward peaked distributions for higher energies. Their conclusion was that a long lived complex, CH_2^+, was an intermediate present at low energies and gives rise to the symmetric forward-backward scattering. The long lifetime of possibly several rotation periods needed for an intermediate to produce symmetric scattering lead Mahan and Sloan[4] to reconsider the C^+ and H_2 reaction. Their experiments confirmed that a triatomic complex is found at low reaction energy. Evidence for this mechanism comes from the lack of large isotope effects[5] expected for direct collision reaction with HD or D_2, and from the large distribution of inelastically scattered C^+ typical of reactions involving imtermediates.

Mahan and Sloan also constructed correlation diagram (shown in Figure 1) from collected data on the states of the separated molecules, atoms, and ions, and the use of elementary molecular orbital theory[6] in order to qualitatively explain their experimental results. As Wolfgang[7] points out, to have an intermediate complex with sufficient lifetime, there must be a deep potential energy well accessible to the reactants and leading to the products. The CH_2^+ species does have a stable $^2A_1$ ground state and a low lying $^2B_1$ excited state,[8] both of which might provide the energy well needed allowing that these states are accessible to the reactants without large energy barriers. The observed threshold energy (0.4 eV) for the $C^+ + H_2 \rightarrow CH^+ + H$ reaction is the same as the expected exothermicity[4] for the reaction, thus ruling out any barrier higher than the ground state products CH^+ and H. Figure 1, represents a best attempt based on experimental observations and elementary molecular orbital theory to explain the correlation of states allowing C^+ and H_2 to reach the low lying CH_2^+ states. In order to make Figure 1 more quantitative, ab-initio electronic structure calculations can be used to calculate the relative positions for the states of CH_2^+ that appear in Figure 1, since surface features like avoided crossings, potential energy barriers, and saddle points are crucial to the discussion of the reaction mechanism.

2. Basis Set and Wavefunctions

The basis set chosen for these calculations is the same "double zeta" contracted gaussian basis used for the CH_2^+ ground and first excited state calculation of Bender and Schaefer.[8] This basis is constructed from Huzinaga's[9] (9s5p) gaussian basis on carbon and his (4s) basis scaled to fit a Slater exponential function with $\zeta = 1.2$ on the hydrogen. Dunning's[10] contractions are used to reduce the atom basis sets to (4s2p) on carbon and (2s) on hydrogen.

Electron correlation is of utmost importance in describing a chemical reaction,[11] because it is necessary to be able to calculate the wavefunction at geometries removed from equilibrium positions. At such geometries the electronic structure is in general changing due to the breaking and forming of chemical bonds. This can be seen for CH_2^+ when the molecule is separated maintaining C_{2v} symmetry to form C^+ and H_2. The ground state electronic structure of CH_2^+ is minimally described by the single determinant wavefunction

$$\Psi(CH_2^+, {}^2A_1) = |1a_1^2\ 2a_1^2\ 1b_2^2\ 3a_1| \quad , \qquad (1)$$

which must change when the carbon ion is separated to become

$$\Psi(C^+({}^2P_u) + H_2({}^1\Sigma_g^+),\ {}^2A_1) = |1a_1^2\ 2a_1^2\ 3a_1^2\ 4a_1| \quad . \qquad (2)$$

For the ${}^2A_1$ reaction surface, configurations (1) and (2) plus the configuration

$$1a_1^2\ 2a_1^2\ 1b_1^2\ 3a_1 \quad , \qquad (3)$$

were combined with all other configurations made from single and double excitations from the occupied orbitals in the configurations (1), (2), and (3) except from the $1a_1$ orbital which was always doubly occupied because it represents the 1s atomic orbital on carbon. The resulting set of 570 configurations was used to calculate the lowest $^2A_1$ potential energy surface for CH_2^+ with C_{2v} symmetry. Similarly the $^2B_1$ and $^2B_2$ potential energy surfaces also originating from $C^+(^2P_u)$ and $H_2(^1\Sigma_g^+)$ constrained to have C_{2v} symmetry are calculated using the $^2B_1$ configurations

$$1a_1^2\ 2a_1^2\ 3a_1^2\ 1b_1 \text{ and } 1a_1^2\ 2a_1^2\ 1b_2^2\ 1b_1 \quad , \qquad (4)$$

representing the $C^+ + H_2$ and CH_2^+ orientations respectively, and the $^2B_2$ configuration

$$1a_1^2\ 2a_1^2\ 3a_1^2\ 1b_2 \quad , \qquad (5)$$

which describes the region of interest by itself. The $^2B_1$ calculation has 380 configurations and the $^2B_2$ has 262 configurations when all single and double excitations (except from $1a_1$) are included.

To complete the $C_{\infty v}$ side of the correlation diagram in Figure 1, where the atoms are constrained to be arranged linear and non-symmetric, the potential energy surfaces for the lowest $^2\Pi$ and $^2\Sigma^+$ states are calculated. The $^2\Pi$ calculation involves the two reference configurations

$$1\sigma^2\ 2\sigma^2\ 3\sigma^2\ 1\pi \quad \text{and} \quad 1\sigma^2\ 2\sigma^2\ 3\sigma\ 1\pi\ 4\sigma \quad , \qquad (6)$$

representing the $C^+(^2P_u) + H_2(^1\Sigma_g^+)$ and $CH(^3\Pi) + H$ orientations respectively, which with their single and double excitations produce 569 configurations. The $^2\Sigma^+$ surface needs only one reference configuration

$$1\sigma^2\ 2\sigma^2\ 3\sigma^2\ 4\sigma \quad , \qquad (7)$$

to minimally describe both $C^+(^2P_u) + H_2(^1\Sigma_g^+)$ and $CH^+(^1\Sigma^+) + H$ orientations, and the single and double excitations combine to make a total of 338 configurations.

A completely general non-symmetric approach of C^+ to H_2 has only C_s symmetry, and the lowest potential energy surface in that case is $^2A'$ symmetry. The $^2A'$ state is minimally described by the configurations

$$1a'^2\ 2a'^2\ 3a'^2\ 4a' \text{ and } 1a'^2\ 2a'^2\ 3a'\ 4a'^2 \quad , \qquad (8)$$

because the 3a' and 4a' orbitals correlate to the $3a_1$ and $1b_2$ orbitals in C_{2v} symmetry and the $^2A'$ potential energy surface should connect the $^2B_2$ and $^2A_1$ surfaces as shown by a dotted line in Figure 1. The reference configurations (8) and their single and double excitations make 648 configurations for the $^2A'$ surface calculation.

The geometry of the CH_2^+ system is specified by the parameters defined in Figures 2-4 depending on the symmetry to which the system is constrained, C_{2v}, $C_{\infty v}$, or C_s. In all cases, $\underline{r}$ is the H-H distance, and for $C_{\infty v}$ and C_s symmetry $\underline{R}$ is the length from C to the nearest H, and for C_{2v} symmetry $\underline{R}$ is the length from C to the H_2 midpoint.

Each point on a potential energy surface represents two calculations. The first is an SCF calculation for the best single configuration wavefunction at that geometry and the orbitals from this calculation are used to start the CI calculation. The natural orbitals[12] from this CI wavefunction are used again as starting orbitals for the CI wavefunction and this is repeated until the energy stabilizes or increases slightly, usually on the second iteration. In the regions where the electronic structure is changing dominant configurations each dominant configuration is used in an SCF calculation to start the CI calculation, and the lowest energy solution is used. In most cases, the SCF configuration with the lowest energy leads to the lowest CI energy.

3. Results

Points on the calculated potential energy surfaces are reported in hartrees for the total energy and in kcal/mole relative to the ground state reactants, C^+ and H_2. Table I shows the total and the relative energies for the stable species represented on the potential energy surfaces. The calculated endothermicity for the reaction $C^+ + H_2 \rightarrow CH^+ + H$ is seen to be 20.8 kcal/mole. Experimentally this endothermicity is the difference of the dissociation energies[13] for CH^+ and H_2, which gives the values 0.44 eV = 10.1 kcal/mole. However, this includes the zero point vibrational energy not included in Table I, so the corrected classical endothermicity becomes 12.5 kcal/mole, and the theoretical result is found to be 8.3 kcal/mole too large.

The product of CH^+ has a low-lying $^3\Pi$ excited state calculated by Green, Bagus, Liu, McLean, and Yoshimine[14] to be 26.3 kcal/mole above the $^1\Sigma^+$ ground state. This calculation has a CH^+ $^1\Sigma^+$-$^3\Pi$ separation of 18.3 kcal/mole, that is 8 kcal/mole below their more accurate calculation.

The important features of the $^2A_1$, $^2B_1$, and $^2B_2$ potential energy surfaces for the C_{2v} symmetric approach of C^+ of H_2 can be seen in Figure 5, and the stationary points are listed in Table II. Figure 5 is an energy profile illustration of the C_{2v} potential energy surfaces where the curves represent minimum energy paths from $C^+ + H_2$ to CH_2^+ for each of the states $^2A_1$, $^2B_1$, and $^2B_2$. This diagram shows several changes from the correlation diagram in Figure 1. The $^2A_1$ surface is still much like Figure 1, but the $^2B_1$ and $^2B_2$ surfaces are very different. For $^2B_2$ symmetry there is no CH_2^+ state lower than C^+ and H_2 so the surface is repulsive, and the $^2B_1$ surface shows a barrier separating C^+ + H_2 from CH_2^+ due to a Woodward and Hoffman[15] avoided crossing. Both the $^2B_1$ and $^2B_2$ surfaces also have long range minima for large C^+ and H_2 separations (see Table II), and the $^2A_1$ surface is initially repulsive.

The saddle points for the $^2A_1$ and $^2B_1$ surfaces were determined by fitting the surface with a bicubic spline function and finding the points on the surface where the partial derivatives in both coordinates are simultaneously zero. For the $^2A_1$ surface this occurs for $R = 2.94$ bohrs and $r = 2.35$ bohrs with an energy 85.7 kcal/mole above the reactants. Likewise, the $^2B_1$ saddle point is at $R = 2.33$ bohrs and $r = 3.00$ bohrs with an energy 62.8 kcal/mole above the reactants. Minimum energy paths near these saddle points are calculated by moving along the steepest gradient direction using reduced mass weighted coordinates.

These pathways are listed in Table III for the $^2A_1$ and $^2B_1$ cases.

Linear non-symmetric $C_{\infty v}$ appraoch of C^+ on H_2 is shown in Figure 6, where the curves are potential energy profiles of mimimum energy paths joining $C^+ + H_2$ and $CH^+ + H$. Only the $^2\Pi$ surface shows a Van der Waals like initial attraction, with a minimum at R = 2.93 bohrs and r = 1.50 bohrs with a well depth of 8.2 kcal/mole. There is no barrier found for the $^2\Pi$ surface which forms excited $^3\Pi$ CH^+ as the product. However, the $^2\Sigma^+$ surface has a saddle point with a barrier height of 28.4 kcal/mole above the reactants and 7.6 kcal/mole above the products at the geometry R = 2.51 bohrs and r = 2.11 bohrs. From Hammond's postulate[16] that the barrier in an endothermic reaction is nearer the products, the 8.3 kcal/mole error in the endothermicity is incorporated into the reactant barrier and the corrected barrier is only 20.1 kcal/mole. It is an interesting result that this barrier occurs where no orbital symmetry is changing, and it would not be predicted by Woodward and Hoffmann's rule.[15] Table IV gives the minimum energy path calculated at the $^2\Sigma^+$ CH_2^+ barrier.

So far, none of the potential energy surfaces examined have explained how the reaction can proceed <u>via</u> the CH_2^+ intermediate, or how the reactants can reach the products without passing a barrier in excess of the endothermicity. To examine these points, the general approach in C_s symmetry is considered for the cases where the C^+ approaches H_2 along the 45^0 and 90^0 paths depicted in Figure 4. In both cases, a saddle point geometry is found for the $^2A'$ ground state surface. The 45^0 angle approach has a saddle point at the geometry R = 2.45 bohrs and r = 2.62 bohrs with a barrier height of 22.9 kcal/mole above the reactants, while the 90^{o} approach has a saddle point at the geometry R = 2.18 bohrs and r = 3.18 bohrs with a barrier energy of 17.8 kcal/mole above the reactants. The 90^{o} approach confirms the expected pathway without a barrier higher than the endothermicity. The $^{2}A'$ surface in C_s symmetry correlates with both the $^{2}A_1$ and $^{2}B_2$ surfaces in C_{2v} symmetry as well as the $^{2}\Sigma^{+}$ and $^{2}\Pi$ surfaces in $C_{\infty v}$ symmetry, (the $^{2}B_1$ C_{2v} surface becomes $^{2}A''$ in C_s symmetry and also correlates to $^{2}\Pi$ in $C_{\infty v}$ symmetry) which means that the $^{2}A'$ surface can access the deep $^{2}A_1$ energy well and the shallow $^{2}B_2$ entry way leading to a crossing with the $^{2}A_1$ surface as seen in Figure 5. The crossing of the $^{2}B_2$ and $^{2}A_1$ surfaces occurs at low relative energies and a segment of this crossing near its minimum energy of 10.3 kcal/mole above the reactants is listed in Table V.

4. Conclusion

The potential energy surface for the reaction $C^{+} + H_2 \rightarrow CH^{+} + H$ has been investigated by ab-initio electronic structure calculations that include most[11] of the valence electron correlation in order to construct a quantitative correlation diagram[6] that can be used to discuss the ion-molecule reaction mechanism. The entire potential energy surface was not calculated here since it would require much more computational effort. Only the regions near features likely to play a part in the correlation diagram in Figure 1 were considered. This work can be used to guide the calculation of a more accurate potential energy surface (using a larger basis set) to the important regions involved in the reaction. However, unless the surface is to be used for dynamics calculations, such an accurate surface is probably not necessary.

The most important feature of the potential energy surface for the $C^+ + H_2 \rightarrow CH^+ + H$ reaction is the $^2B_2$ and $^2A_1$ surface intersection which becomes an avoided crossing in C_s symmetry allowing the reactants access to the $^2A_1$ energy well at the CH_2^+ ground state. Of additional interest is the $^2\Sigma^+$ energy barrier which does not result from a change in orbital symmetry.

REFERENCES

1. W. B. Maier, J. Chem. Phys. 46, 4991 (1967).
2. C. R. Iden, R. Liardon, and W. S. Koski, J. Chem. Phys. 54, 2757 (1971).
3. C. R. Iden, R. Liardon, and W. S. Koski, J. Chem. Phys. 56, 851 (1972).
4. B. H. Mahan and T. M. Sloan, J. Chem. Phys. 59, 5661 (1973).
5. B. H. Mahan, Acc. Chem. Res. 1, 217 (1968).
6. B. H, Mahan, J. Chem. Phys. 55, 1436 (1971).
7. R. Wolfgang, Acc. Chem. Res. 3, 48 (1970).
8. C. F. Bender and H. F. Schaefer, III, J. Mol. Spect. 37 423 (1971).
9. S. Huzinaga, J. Chem. Phys. 42, 1293 (1965).
10. T. H. Dunning, J. Chem. Phys. 53, 2823 (1970).
11. H. F. Schaefer, III, The Electronic Structure of Atoms and Molecules: A Survey of Rigorous Quantum Mechanical Results, Addison Wesley, Reading, Massachusetts, 1972.
12. P.-O. Löwdin, Phys. Rev. 97, 1474 (1955).
13. $D_o(CH^+) = 4.04$ eV, $D_e(CH^+) = 4.21$ eV, from G. Herzberg and J. W. C. Johns, Astrophys. J. 158, 399 (1969), $D_o(H_2) = 4.48$ eV, $D_e(H_2) = 4.75$ eV, from W. Kolos and L. Wolniewicz, J. Chem. Phys. 49, 404 (1968).
14. S. Green, P. S. Bagus, B. Liu, A. D. McLean, and M. Yoshimine, Phys. Rev. A 5, 1614 (1972).
15. R. B. Woodward and R. Hoffman, The Conservation of Orbital Symmetry, Verlag Chemie (1971).

Table I. Energies of Stationary Species in the Reaction

$C^+ + H_2 \rightarrow CH^+ + H$

Species	Total Energy (hartrees)	Energy above Reactants (kcal/mole)
$C(^2P_u) + H_2(^2\Sigma_g^+)$	-38.4843	0.0
$CH_2(^2A_1)$	-38.6152	-82.1
$CH_2(^2B_1)$	-38.6104	-79.1
$CH(^1\Sigma^+) + H$	-38.4514	20.8
$CH(^3\Pi) + H$	-38.4221	39.0

Table II. Stationary points on the CH_2 potential energy surfaces. Energies are in kcal/mole relative to the reactants C^+ and H_2 and also in hartrees. Bond distances are in bohr (1 bohr = 0.529177Å).

Surface	Geometry R	Geometry r	Nature	Energy
$^2A_1$	2.94	2.34	Saddle Point	85.7 (-38.3479)
$^2B_1$	3.66	1.46	Long Range Attraction	-7.3 (-38.4959)
$^2B_1$	2.33	3.00	Saddle Point	62.8 (-38.3842)
$^2B_2$	3.34	1.49	Long Range Attraction	-8.3 (-38.4975)
$^2\Sigma^+$	2.51	2.11	Saddle Point	28.4 (-38.4390)
$^2\Pi$	2.93	1.50	Long Range Attraction	-8.2 (-38.4974)
$^2A'(45^o)$	2.45	2.62	Saddle Point	22.9 (-38.4478)
$^2A'(90^o)$	2.18	3.18	Saddle Point	17.8 (-38.4628)

Table III. C_{2v} minimum energy paths near the saddle point for $C^+ + H_2 \rightarrow CH_2^+$. Bond distances are given in bohrs and energies in kcal/mole relative to separated $C^+ + H_2$.

$C^+ + H_2 \rightarrow {}^2A_1\ CH_2^+$

R(C - X)	r(H - H)	Energy	Comments
∞	1.40	0.0	Reactants
2.96	2.07	76.8	
2.95	2.21	82.1	
2.95	2.30	84.5	
2.94	2.34	85.6	Saddle Point
2.89	2.34	85.4	
2.87	2.39	84.0	
2.85	2.52	77.6	
2.83	2.57	74.5	
0.71	3.93	-82.1	
			Product

$C^+ + H_2 \rightarrow {}^2B_1\ CH_2^+$

R(C -X)	r(H - H)	Energy	Comments
∞	1.40	0.0	Reactants
2.51	2.54	47.9	
2.43	2.74	56.7	
2.38	2.87	61.1	
2.33	3.00	62.8	Saddle Point
2.26	3.05	61.6	
2.20	3.13	58.4	
2.11	3.20	51.9	
0.00	4.16	-79.1	
			Product

Table IV. $^2\Sigma^+$ minimum energy path for $C^+ + H_2 \rightarrow CH^+ (^1\Sigma^+) + H$ near the saddle point. Bond distances are in bohrs and energies in kcal/mole relative to separated $C^+ + H_2$.

R(C - H)	r(H - H)	Energy	Comments
∞	1.40	0.0	Reactants
2.87	1.42	20.4	
2.71	1.64	24.1	
2.57	1.95	27.9	
2.51	2.11	28.4	Saddle point
2.46	2.27	27.9	
2.41	2.41	27.1	
2.17	∞	20.8	Products

Table V. $^2A_1$ and $^2B_2$ surface intersection near its minimum for the process $C^+ + {}^1H_2 \rightarrow CH_2^+$. Energies are given in kcal/mole above the reactants C^+ and H_2, lengths are in bohrs.

R	r	Energy
2.00	2.18	12.4
2.03	2.24	11.2
2.06	2.32	10.4
2.09	2.39	10.3
2.12	2.46	10.4
2.15	2.53	10.8
2.18	2.60	11.6
2.21	2.86	12.6
2.24	2.76	13.8

FIGURE CAPTIONS

Figure 1. Molecular orbital theory state correlation diagram devised by Mahan and Sloan, Ref. 4. States for C_{2v} symmetry are on the left side and $C_{\infty v}$ on the right side.

Figure 2. C_{2v} geometry parameters.

Figure 3. $C_{\infty v}$ geometry parameters.

Figure 4. C_s geometry parameters.

Figure 5. C_{2v} energy profiles for minimum energy paths viewed along the r coordinate.

Figure 6. $C_{\infty v}$ energy profiles for minimum energy paths viewed along the r coordinate.

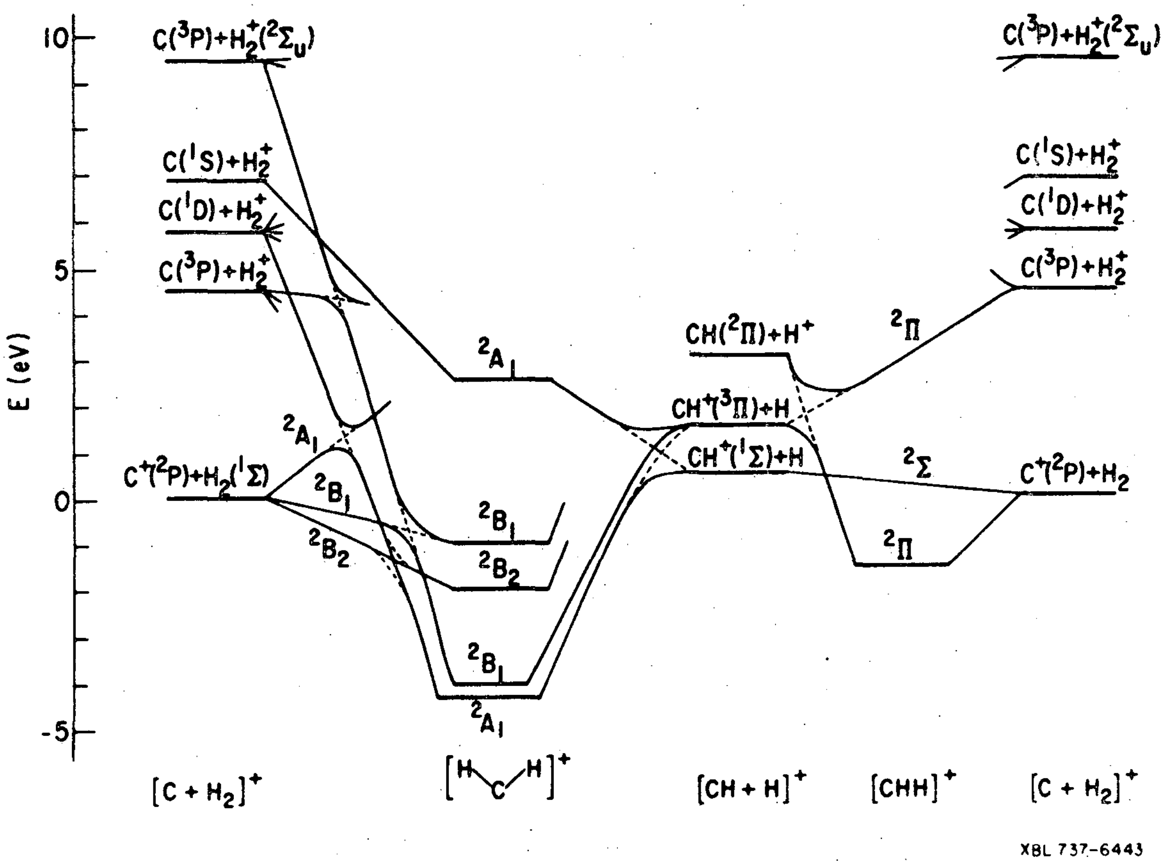
E (eV)
10
5
0
-5
C(³P)+H₂⁺(²Σu)
C(¹S)+H₂⁺
C(¹D)+H₂⁺
C(³P)+H₂⁺
C⁺(²P)+H₂(¹Σ)
²A₁
²B₁
²B₂
CH(²Π)+H⁺
CH⁺(³Π)+H
CH⁺(¹Σ)+H
²Π
²Σ
C⁺(²P)+H₂
[C + H₂]⁺
[CH + H]⁺
[CHH]⁺
XBL 737-6443

Figure 1

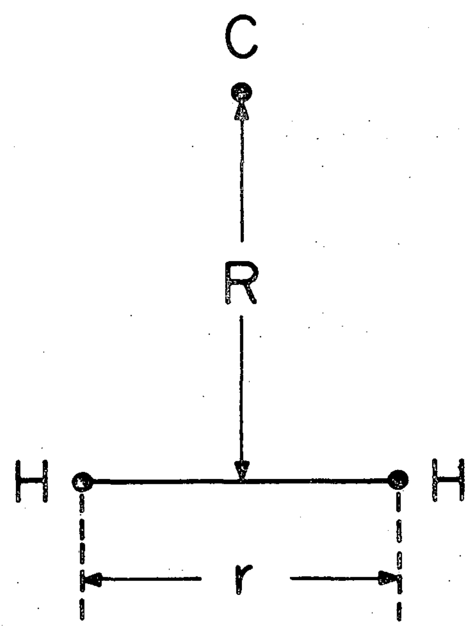

C_{2v} Geometries

XBL739-4046

Figure 2

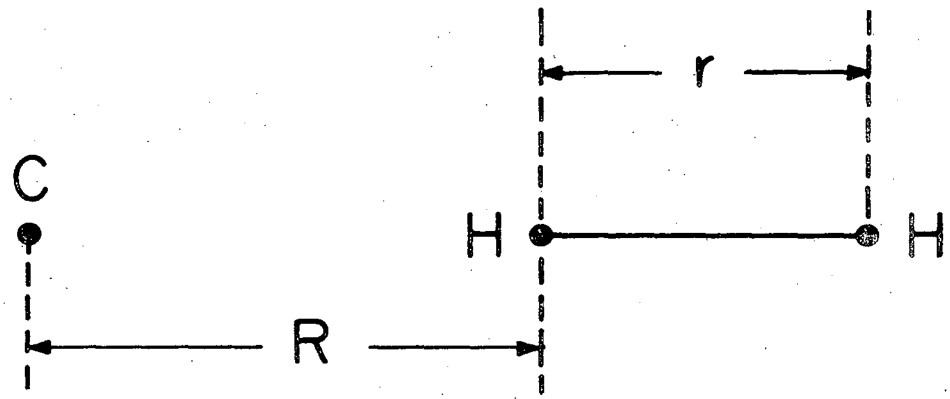

$C_{\infty v}$ Geometries

XBL739-4045

Figure 3

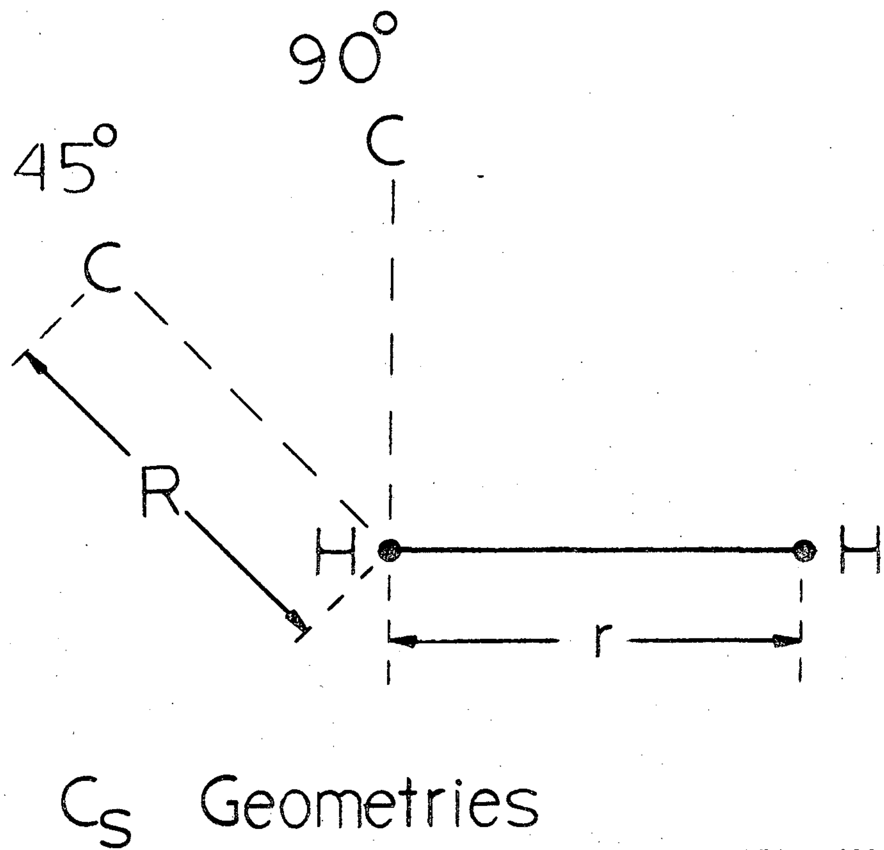

XBL 748-1428

Figure 4

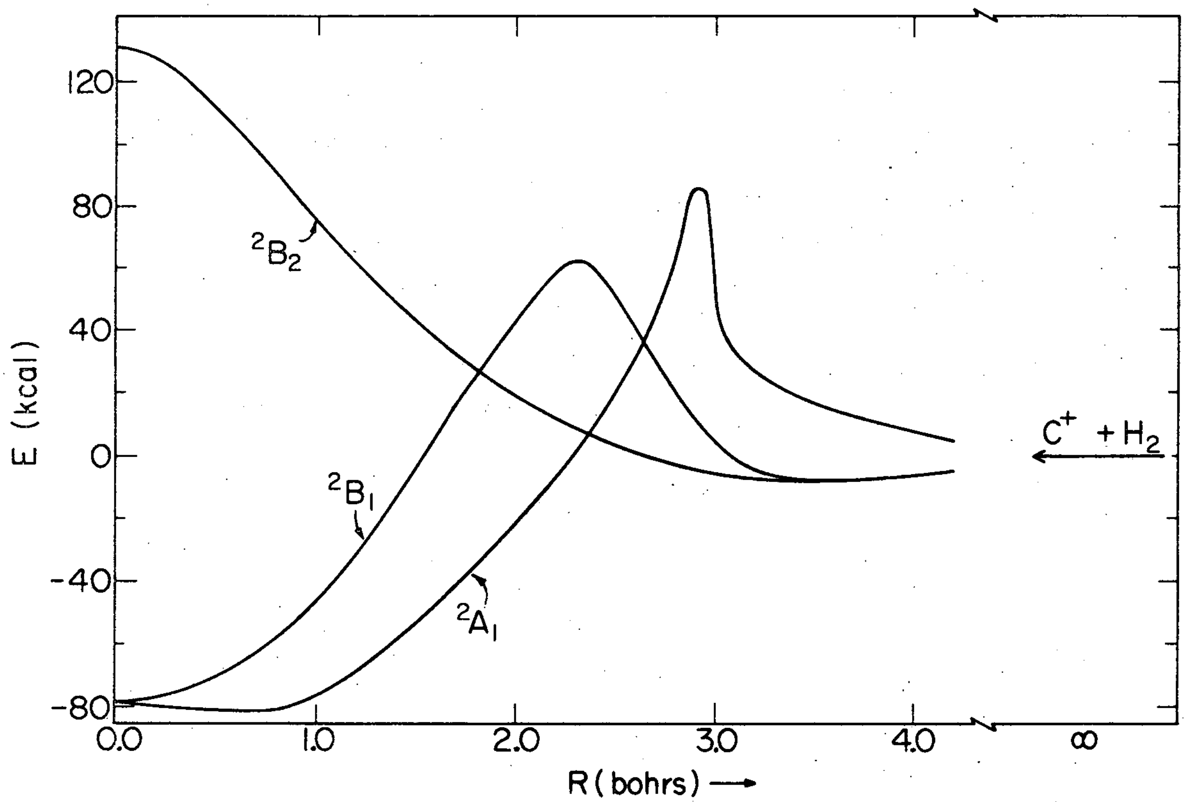

XBL 7310-4163

Figure 5

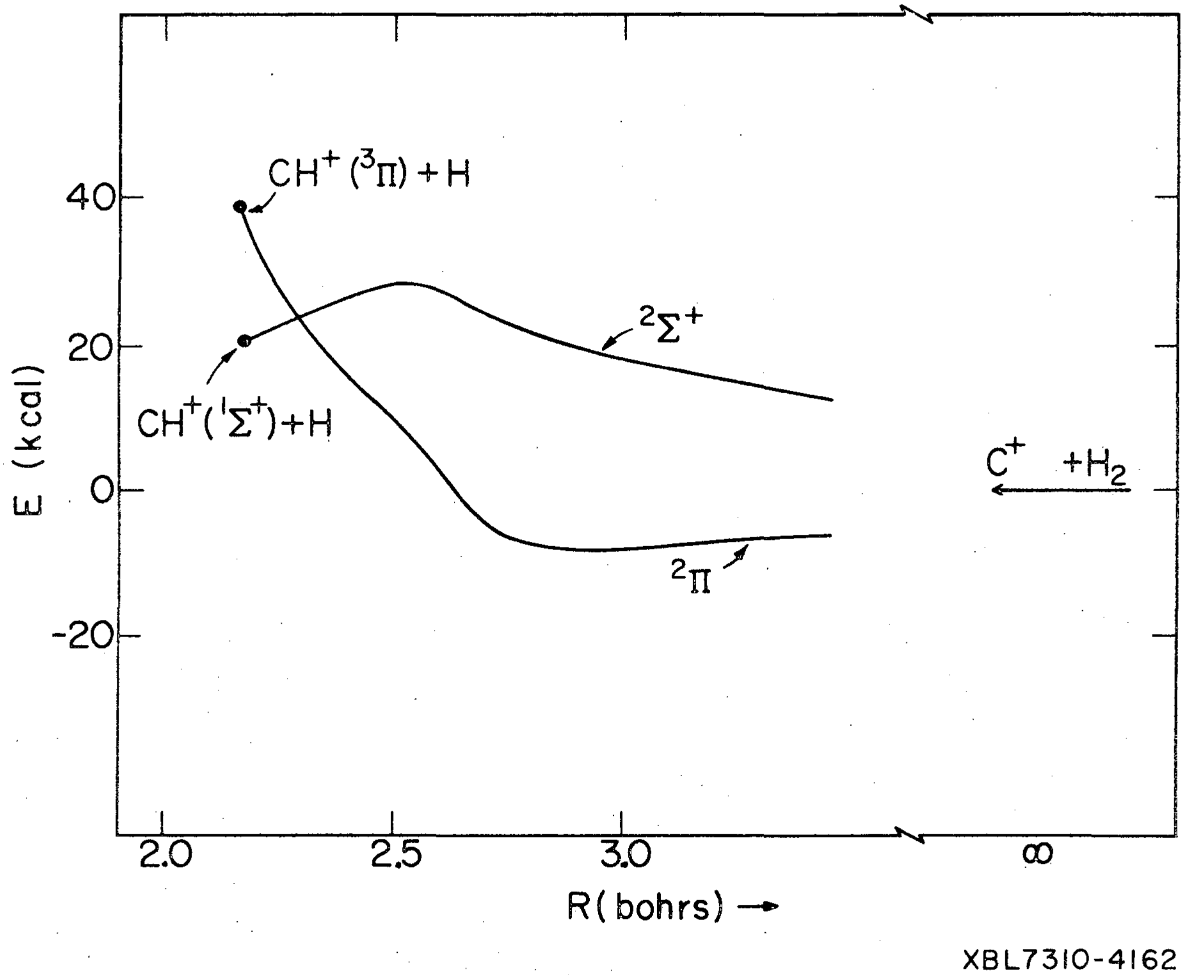
CH+ (3Π) + H
CH+(1Σ+)+H
2Σ+
2Π
C+ +H2
40
20
0
-20
E (kcal)
2.0
2.5
3.0
∞
R(bohrs)
XBL7310-4162

Figure 6

ACKNOWLEDGMENTS

This thesis contains the fruits of my four years at Berkeley and is, in part, possible because of the shared wisdom and guidance of my research advisor, Professor Henry F, Schaefer III. The useful configuration interaction program used in my work was CIMOL, a program written and developed by Dr. Charles F. Bender, who provided his program for our use. Other counsel and encouraging friendship came from my fellow researchers Steven V. O'Neil, Peter K. Pearson, David R. Yarkony, Barbara J. Garrison, Gretchen M. Schwenzer, and Charles W. Bauschlicher. And on top of all that, this work was performed under the auspices of the U. S. Atomic Energy Commission.

TECHNICAL INFORMATION DIVISION
LAWRENCE BERKELEY LABORATORY
UNIVERSITY OF CALIFORNIA
BERKELEY, CALIFORNIA 94720